# Severe allergic dysregulation due to a gain of function mutation in the transcription factor STAT6

Safa Baris, MD,[a,b,c]* Mehdi Benamar, PhD,[d,e]* Qian Chen, PhD,[d,e] Mehmet Cihangir Catak, MSc,[a,b,c] Mónica Martínez-Blanco, PhD,[d,e] Muyun Wang, BA,[d,e] Jason Fong, BSc,[d,e] Michel J. Massaad, PhD,[f,g] Asena Pinar Sefer, MD,[a,b,c] Altan Kara, PhD,[h] Royala Babayeva, MD,[a,b,c] Sevgi Bilgic Eltan, MD,[a,b,c] Ayse Deniz Yucelten, MD,[i] Emine Bozkurtlar, MD,[j] Leyla Cinel, MD,[j] Elif Karakoc-Aydiner, MD,[a,b,c] Yumei Zheng, PhD,[k,l] Hao Wu, PhD,[k,l] Ahmet Ozen, MD,[a,b,c] Klaus Schmitz-Abe, PhD,[d,e,m] and Talal A. Chatila, MD, MSc[d,e] *Istanbul and Gebze, Turkey; Boston, Mass; and Beirut, Lebanon*

## GRAPHICAL ABSTRACT

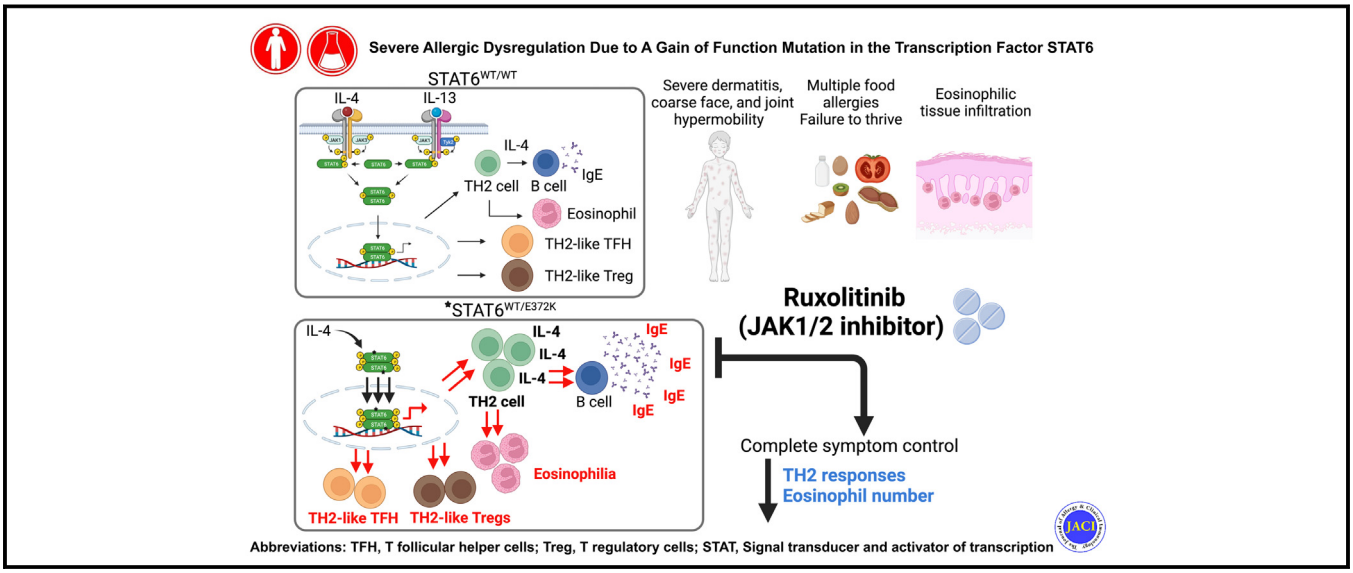


**Background: Inborn errors of immunity have been implicated in causing immune dysregulation, including allergic diseases. STAT6 is a key regulator of allergic responses.**

**Objectives: This study sought to characterize a novel gain-of-function STAT6 mutation identified in a child with severe allergic manifestations.**

**Methods: Whole-exome and targeted gene sequencing, lymphocyte characterization, and molecular and functional analyses of mutated STAT6 were performed.**

**Results: This study reports a child with a missense mutation in the DNA binding domain of STAT6 (c.1114G>A, p.E372K) who presented with severe atopic dermatitis, eosinophilia, and elevated IgE. Naive lymphocytes from the affected patient displayed increased $T_H2$- and suppressed $T_H1$- and $T_H17$-cell responses. The mutation augmented both basal and cytokine-induced STAT6 phosphorylation without affecting dephosphorylation kinetics. Treatment with the Janus kinase 1/2 inhibitor ruxolitinib reversed STAT6 hyperresponsiveness to IL-**

From [a]the Division of Pediatric Allergy and Immunology and the Departments of [i]Dermatology and [j]Pathology, School of Medicine, Marmara University, [b]the Istanbul Jeffrey Modell Diagnostic and Research Center for Primary Immunodeficiencies, and [c]The Isil Berat Barlan Center for Translational Medicine, Istanbul; [d]the Division of Immunology, [l]Program in Cellular and Molecular Medicine, and [m]The Manton Center for Orphan Disease Research, Boston Children's Hospital and the Departments of [e]Pediatrics and [k]Biological Chemistry and Molecular Pharmacology, Harvard Medical School, Boston; [f]the Department of Experimental Pathology, Immunology, and Microbiology, American University of Beirut and [g]the Department of Pediatrics and Adolescent Medicine, American University of Beirut Medical Center; and [h]the TUBITAK Marmara Research Center, Gene Engineering and Biotechnology Institute, Gebze.

*These authors contributed equally to this work.

Supported by grants from the National Institutes of Health (NIH R01AI128976 and R01AI126915 to T.A.C.), Scientific and Technological Research Council of Turkey (318S202 to S.B.), and the Office of Faculty Development at Boston Children's Hospital (to M.B.).

Disclosure of potential conflict of interest: The authors declare the they have no relevant conflicts of interest.

Received for publication September 21, 2022; revised January 20, 2023; accepted for publication January 26, 2023.

Corresponding author: Talal A. Chatila, MD, MSc, Division of Immunology, Boston Children's Hospital, Department of Pediatrics, Harvard Medical School, Boston, MA 02115, USA. E-mail: talal.chatila@childrens.harvard.edu.

0091-6749/$36.00



https://doi.org/10.1016/j.jaci.2023.01.023

**4, normalized $T_H1$ and $T_H17$ cells, suppressed the eosinophilia, and improved the patient's atopic dermatitis.**
**Conclusions: This study identified a novel inborn error of immunity due to a STAT6 gain-of-function mutation that gave rise to severe allergic dysregulation. Janus kinase inhibitor therapy could represent an effective targeted treatment for this disorder. (J Allergy Clin Immunol 2023;■■■:■■■-■■■.)**

***Key words:*** *Inborn errors of immunity, primary atopic disorders, STAT6, gain-of-function mutation, Janus kinase inhibitors, Jakinibs*

*Abbreviations used*
AD: Atopic dermatitis
APC: Allophycocyanin
CRTH2: Chemoattractant receptor homologous molecule expressed on $T_H2$-type cells
$cT_{FH}$: Circulating follicular helper T
GFP: Green fluorescent protein
GOF: Gain-of-function
HIES: Hyper IgE syndrome
IEI: Inborn errors of immunity
IL-4R: IL-4 receptor
JAK: Janus kinase
Jakinibs: JAK inhibitors
p: Phosphorylated
SH2: Src homology 2
STAT: Signal transducer and activator of transcription
Treg: Regulatory T
WES: Whole-exome sequencing
WT: Wild type

A number of monogenic inborn errors of immunity (IEI) give rise to allergic dysregulation as a prominent disease manifestation.[1,2] Originally, heterozygous loss-of-function mutations in STAT3 were first identified as the cause of autosomal dominant form of the hyper IgE syndrome (HIES).[3] Afterward, DOCK8 deficiency was discovered to cause the autosomal recessive form of the disease.[4,5] Subsequently, other genetic causes of HIES have been identified, encompassing mutations in *PGM3*, *ZNF341*, *IL6ST*, *IL6R*, *ERBIN*, *TGFBR1*, *TGFBR2,* and *CARD11*.[6-10] Recently, pertaining to IEI disorders with atypical allergic manifestations, the term "primary atopic disorders" has emerged to unify these disorders under 1 umbrella,[9,11] encompassing >35 monogenetic disorders.[2,8] Gain-of-function (GOF) mutations in Janus kinase (JAK)–signal transducer and activator of transcription (STAT) signaling pathways have also been associated with atopic manifestations,[12] including ones targeting *STAT3*, *STAT5B,* and *JAK1*.[13-16]

STAT6 is the central transcription factor that mediates the biological effects of IL-4 and IL-13.[17-19] The binding of IL-4 and IL-13 to IL-4R receptor (IL-4R) complexes triggers the phosphorylation of conserved tyrosine residues in the cytoplasmic domain of the common IL-4 receptor alpha (IL-4Rα) subunit by the receptor-associated JAKs.[20,21] STAT6 is subsequently recruited through the binding of its tandem Src homology 2 (SH2) domains to the IL-4Rα phosphotyrosine docking sites.[22] Once bound to the receptor, STAT6 is phosphorylated by the JAKs, resulting in its dimerization via the SH2 domains and its translocation into the nucleus, where it activates the expression of target genes by binding to a specific DNA sequence motif.[23,24]

The IL-4R-STAT6 axis plays a critical role in type 2 immunity by directing protective responses to parasites and toxins; promoting B-cell development, activation, and class switching to IgE and $IgG_1$; and directing overall tissue repair.[22,25,26] For the same reasons, its dysregulation plays a pathogenic role in different allergic diseases.[27] STAT6 signaling promotes the differentiation of $T_H2$ cells by upregulating the expression of the master transcriptional regulator GATA3.[28,29] Furthermore, STAT6 signaling renders $T_H2$ cells resistant to regulatory T (Treg) cell–mediated suppression,[30] while excessive STAT6 signaling in Treg cells results in their acquisition of a $T_H2$ cell–like phenotype that contributes to the allergic response.[31] STAT6 single nucleotide polymorphisms are associated with increased serum IgE, eosinophil, food allergy, and asthma.[32,33] Exaggerated STAT6 activity due to somatic *STAT6* mutations is often linked to malignancies, especially Hodgkin and non-Hodgkin lymphomas.[34,35] A transgenic mouse model (STAT6VT) expressing a lymphoid tissue–restricted constitutively active STAT6 GOF variant created by introducing mutations in the SH2 domains exhibited an IL-4–independent augmented $T_H2$-cell response. These mice developed atopic dermatitis (AD)-like phenotype with blepharitis and allergic lung inflammation.[36,37] In line with the known critical function of IL-4R–STAT6 axis in the initiation and promotion of $T_H2$ responses, we herein report a patient with germline sporadic GOF mutation in *STAT6* as the molecular etiology of a previously unknown syndromic HIES. We showcase the impact of perturbations in T-cell responses downstream of altered STAT6 signaling and deliver proof of concept for improving immune cell activation and differentiation in patient cells by JAK inhibitors (Jakinibs).

## METHODS

### Clinical assessments

The local ethics committees from Marmara University and Boston Children's Hospital approved the clinical and research studies' protocol, and written informed consent was obtained from the patient family and control subjects. We documented the clinical and demographic features of the patient and provided data regarding long-term follow-up.

### Antibodies and flow cytometry

To determine detailed lymphocyte subsets, the following mAbs were used: fluorescein isothiocyanate–conjugated CD3 (UCHT1; Beckman Coulter, Indianapolis, Ind), allophycocyanin (APC)-Alexa Fluor 700 CD4 (13B8.2, Beckman Coulter), Krome Orange CD45 (J33, Beckman Coulter), APC–Alexa Fluor 750 CD45RA (2H4DH11LDB9, Beckman Coulter), phycoerythrin-cyanin 7 CD8 (SFCI21Thy2D3, Beckman Coulter), phycoerythrin-Texas red-x CD45RO (UCHL1, Beckman Coulter), phycoerythrin-cyanin 5.5 CD25 (B1.49.9, Beckman Coulter), Alexa Fluor 647 Foxp3 (259D; BD Biosciences, San Jose, Calif), phycoerythrin P-STAT6 (A15137E; BioLegend, San Diego, Calif), fluorescein isothiocyanate CRTH2 (BM16, BioLegend), APC-Gata3 (16E10A23, BioLegend), BV605 CCR4 (L291H4, BioLegend), phycoerythrin RORγt (Q31-378, BD Biosciences), CD27 (0323, BioLegend), CD19 (4G7, BioLegend), CD23 (EBVCS-5, BioLegend), IgE (MHE-18, BioLegend), IgD (IA6-2, BioLegend), CD38 (HB-7, BioLegend), CD20 (2H7, BioLegend). Peripheral blood lymphocyte subset analyses, upregulation, and proliferation assays were performed by flow cytometry as described previously.[38-40] For lymphocyte subset analysis, 100 μL of whole blood was incubated with mAbs against surface markers for 20 minutes in the dark at room temperature. Red cells were lysed and washed before acquisition. For visualization of Treg cells, after isolation of PBMCs, the cells were fixated and

permeabilized, followed by overnight incubation for intracellular Foxp3 staining. All stained cells were acquired with a Navios EX cytometer (Beckman Coulter) and analyzed with Kaluza Analysis Software (version 2.1, Beckman Coulter). CD25 upregulation and proliferation assay were performed by isolation of PBMCs and stimulation in anti-CD3/anti-CD28 (1 μg/mL each) 96-well plates for 3 days, following labeling with CellTrace Violet (Thermo Fisher Scientific, Waltham, Mass) according to manufacturer's instructions. CD69 upregulation was evaluated after 24 hours of stimulation with anti-CD3/anti-CD28 (1 μg/mL each). For intracellular IL-4, IL-17A, IL-10, and IFN-γ detection, cell suspensions ($1 \times 10^6$ cells) were incubated with protein transport inhibitor containing monensin (BD Bioscience), phorbol 12–myristate 13–acetate (50 ng/mL), and ionomycin (1 μg/mL) for 6 hours. After incubation, cells were fixed. For intracellular cytokine staining, fixed cell pellets were resuspended in permeabilization reagent containing saponin (Thermo Fisher Scientific), mixed with fluorescent-labeled cytokine-specific antibody. After 45 minutes of incubation, cells were washed twice and cell surface staining was performed with fluorescent-labeled antibodies against CD4, CD45RA, and CD45RO. Stained cells were acquired by Navios EX cytometer and analyzed by FlowJo software (TreeStar, Ashland, Ore). For analysis of phosho(p)-STATs by phosphoflow, total PBMCs from either healthy controls or patient pre- and posttreatment were stimulated at 37°C in nonsupplemented RPMI 1640 with IL-4 (20 ng/mL), IL-2 (10 ng/mL), or IL-6 (20 ng/mL). For the STAT6 dephosphorylation following cytokine withdrawal, cells were washed with RPMI after stimulation with IL-4 and incubated in RPMI at 37°C and examined for p-STAT6 levels at 0-30 minutes, as previously described for STAT1 GOF mutations.[41,42] Reactions were stopped and cells were permeabilized using a Foxp3/transcription factor staining buffer (eBioscience, San Diego, Calif) and Perm buffer III (BD Biosciences). Cells were stained using phycoerythrin anti pY641-STAT6 (A15137E, BioLegend), APC anti-pY694-STAT5 (A17016B.Rec, BioLegend), Efluor450 Foxp3 (236A/E7, Thermo Fisher Scientific), APC–cyanin 7 CD3 (OKT3, BioLegend), BV785 CD4 (OKT4, BioLegend), and/or BV605 CD8 (HIT8a, BioLegend) mAbs. Samples were acquired on a Fortessa cytometer (BD, Franklin Lakes, NJ), and data were analyzed using the FlowJo software.

## *In vitro* B-cell IgE class switching assay

$CD19^+IgD^+CD27^-CD23^-IgE^-$ naive B cells were purified by fluorescent-activated cell sorting and cultured *in vitro* for 4 days at 30,000 cells per tissue culture plate well in the presence of either an $IgG_1$ isotype control antibody (0.5 μg/mL; 400165,BioLegend) or with an anti-CD40 mAb (0.5 μg/mL, 334350, BioLegend)+IL-4 (20 ng/mL, PeproTech, Rocky Hill, NJ). At the end of the culture period the cells were stained with a viability dye and anti-CD19, -CD27, -CD23, and -IgE mAbs and analyzed by flow cytometry.

## ELISA for human total IgE

The levels of IgE in cells supernatants were determined by sandwich ELISA, and 96-well plates were coated with 2 μg per well of Purified Mouse Anti-Human IgE (BD Biosciences). For the standard curve, Chimeric Human IgE anti NP (Bio-Rad Laboratories, Hercules, Calif) was used. The supernatants were incubated at 4°C overnight, followed by a detection antibody incubation step with Goat anti-Human IgE Fc Secondary Antibody, horseradish peroxidase (Thermo Fisher Scientific). The reaction was developed using TMB as substrate (Thermo Fisher Scientific) and read at 450 nm.

## Generation of STAT6 variant plasmids and expression of STAT6 variants

A plasmid used for transfection studies contained full-length STAT6 in a pCMV6 entry vector with a C-terminal green fluorescent protein (GFP) tag (pCMV6-AC-STAT6-GFP) that was purchased from OriGene Technologies (RG210065; Rockville, Md). The directed STAT6 mutagenesis (c.G1114A; p.E372K) plasmid was generated with standard cloning techniques by using pCMV6-AC-STAT6-GFP as a template. Transient expression of STAT6 variants in HEK293T cells were accomplished using GeneJuice transfection reagent (Merck Millipore, Burlington, Mass) according to manufacturer's recommendations. Briefly, the day before transfection, HEK293T cells were seeded at a density of $5 \times 10^5$ cells per well in 6-well plates in 3-mL Dulbecco modified Eagle medium with 10% FBS (Gibco, Life Technologies; Rockville, Md) and incubated for 24 hours at 37°C. The next day, HEK293T cells were transiently transfected with 2 μg of either pCMV6-AC-STAT6-GFP wild-type (WT) or STAT6 mutant plasmid using GeneJuice transfection reagent. Cells were harvested 24 hours after transfection for phosphoflow cytometry analysis.

## Luciferase reporter assays

The p4xSTAT6-Luc2P luciferase reporter plasmid encoding 4xSTAT6 binding sites [TTCCCAAGAA] was obtained from Addgene (35554; Watertown, Mass) and used to assess STAT6 promoter activity. The pRL-SV40 Renilla luciferase control reporter vector was obtained from Promega (E2261; Madison, Wis) and was used in cotransfection studies with p4xSTAT6-Luc2P for internal normalization. HEK293 cells were seeded in 96-well plates overnight at a density of 30,000 cells per well and transfected with 20 ng of plasmids encoding either GFP-tagged WT or p.E372K STAT6. The cells were further transfected with 100 ng of p4xSTAT6-Luc2P and 4 ng the pRL-SV40 vectors using Fugene HD transfection reagent (E2311, Promega), according to manufacturer's recommendations. The next day, transfected cells were stimulated with 100 ng/mL of IL-4 (200-04, PeproTech), and transfected but otherwise untreated cells were used as a control group. Firefly and Renilla luciferase activities, as indicated by relative luminescence units, were determined using Dual-Glo luciferase assay kits (E2920, Promega), according to the manufacturer's instructions. Luciferase activity was measured on BioTek Synergy HTX Multi-Mode Microplate Reader (Agilent Technologies, Santa Clara, Calif).

## Immunofluorescence imaging

Confocal microscopic analysis of STAT6 and p-STAT6 nuclear translocation was carried out following previously described methods.[43] HEK293T cells were grown on the coverslips and transfected with indicated plasmid. After stimulation with 100 ng/mL of IL-4 for 1 and 4 hours, the cells were fixed for 20 minutes in 4% paraformaldehyde and permeabilized with 0.3% Triton X-100. After blocking with 5% BSA, the cells were stained with a mouse anti-p-STAT6 mAb [clone 4H253, sc71793; Santa Cruz Biotechnology, Dallas, Tex) and anti-STAT6 rabbit mAb (clone D3H4, 5397; Cell Signaling Technology, Danvers, Mass), incubated at 4°C overnight. Alexa Fluor 555-goat anti-mouse $IgG_1$ (A21127; Invitrogen, Thermo Fisher Scientific) and Alexa Fluor Plus-647 conjugated goat anti-rabbit (A32733, Invitrogen) secondary antibodies (1:500 dilution) were used for visualizing. Afterward, cells were washed with PBS and stained with 4′-6-diamidino-2-phenylindole, dihydrochloride (1:10,000 dilution; Sigma, St Louis, Mo). Images were acquired with a Zeiss LSM880 confocal microscope (Oberkochen, Germany) and ZEN imaging software (Zeiss). Ten fields were selected randomly and total cells in the field were analyzed for the percentage of STAT6 nuclear localization using ImageJ software (National Institutes of Health, Bethesda, Md).

## Whole exome sequencing

The genetic diagnosis was made by whole-exome sequencing (WES) and the detected variant was confirmed by Sanger sequencing. Briefly, genomic DNA was extracted from peripheral blood samples and 1 μg of DNA was used for exome capture using the IDT XGen exome target design (Integrated DNA Technologies, Coralville, Iowa) or Agilent SureSelect Human All Exon. Generated libraries were sequenced using 75-bp paired-end sequencing on an Illumina NovaSeq-6000 (San Diego, Calif) and BGISeq-500 platform (BGI Genomics, Cambridge, Mass). Captured fragments were sequenced to achieve a minimum of 85% of the target bases covered at 20× or greater coverage. Analysis of WES data was performed using "Variant Explorer Pipeline" to narrow down potential candidate variants.[44] Raw data were processed, filtered, and analyzed according the Variant Explorer Pipeline

recommendations. Candidate genes were further evaluated by our research team (see Table E1 in this article's Online Repository at www.jacionline.org). Sanger sequencing was performed to confirm the mutation identified by the WES. Briefly, genomic DNA was amplified by PCR and amplimers were sequenced using the Big Dye Terminator v1.1 Cycle Sequencing Kit (Applied Biosystems, Life Technologies, Darmstadt, Germany) on an Applied Biosystems 3130 Genetic Analyzer.

### Statistical analysis

The data are expressed as mean and SEM. Analysis of luciferase reporter activity, p-STAT6 phosphorylation, and p-STAT6 nuclear translocation in HEK293 cells was carried out using 2-way ANOVA with posttest analysis. Differences in values were considered significant at $P < .05$.

## RESULTS

### Identification of a novel STAT6 mutation ($STAT6^{E372K}$) causing severe allergy dysregulation

The index case is a 10-year-old boy born to consanguineous parents. He presented in the newborn period with severe atopic eczema, incessant itching, severe growth retardation, generalized lymphadenopathy, and pneumonia. He had generalized skin rash since the newborn period and itching was severely affecting his quality of life. Eczema and itching did not benefit from any local therapies and oral antihistamines. The eczema was associated with a robust IgE response to aero- and food allergens, including high levels of specific serum IgE to mite, grass, wheat, soy, cow milk, egg, tomato, kiwi, almond, and nuts. He experienced urticaria after ingestion of kiwi and almond, and he displayed dysphagia with vomiting following intake of wheat products, egg white, and tomato. A skin biopsy was performed at the age of 7 years that revealed chronic dermal inflammation characterized by perivascular and perifollicular eosinophils, follicular mucinosis, and fibrosis (Fig 1, *A*). During this period, the patient developed generalized lymphadenopathy involving the cervical, axillary, and inguinal lymph node, which persisted despite antibiotic therapy, prompting screening for malignancy. A bone marrow aspirate and biopsy were normal. An inguinal lymph node biopsy revealed findings consistent with reactive follicular hyperplasia and paracortical enlargement. Meanwhile, he developed fever and painful swellings in his skin and axillary lymph nodes, and an ultrasound detected a local tissue abscess. *Staphylococcus aureus* was isolated and was treated with a systemic anti-staphylococcal antibiotic regimen.

One year later, he was admitted to the hospital with a fever and cough. Chest x-ray showed pneumonia and parapneumonic effusion. Methicillin resistance *S aureus* was detected in his sputum and blood cultures. Lung computed tomography revealed ground-glass densities and interlobular septal thickenings, predominantly in the peripheral and paramediastinal parts of both lungs. On physical examination, his weight (18 kg) and height (118 cm) were below the third percentile and he had mild developmental delay. There were xerotic excoriated lichenified eczematous lesions covering all the body, accompanied by hyperpigmentation. Coarse facial appearance with broad nasal bridge, increased alar width, and deep-set eyes; mild high palate arch; hyperextensibility; digital clubbing; and enlarged cervical, axillary, and inguinal lymph nodes were also notable. He had normal dentition but with enamel hypoplasia (see Fig E1 in this article's Online Repository at www.jacionline.org). The SCORAD (SCORing Atopic Dermatitis) and National Institute of Health–HIES scores were 96 and 44; respectively[45,46] (see Table E2 in this article's Online Repository at www.jacionline.org). Nevertheless, he had no evidence of AD-HIES–associated pneumatocele formation or vascular anomalies as evidenced by normal lung computed tomography, brain magnetic resonance imaging, and angiography. He was commenced on prophylactic antibiotic therapy and intravenous immunoglobulin replacement. Due to difficulty in swallowing, we performed upper and lower gastrointestinal endoscopy and showed findings of esophagitis and colitis with mild eosinophilic infiltrations (Fig 1, *A*). The endocrinologic evaluation revealed growth hormone deficiency (growth hormone: 0.93 mIU/L [range 5.4-10.3], insulin-like growth factor 1: 72 μg/L [range 85.7-343]), and he was scheduled to start growth hormone replacement therapy.

His immunologic workup was particularly notable for persistent eosinophilia (3,100 eosinophils per $mm^3$). He had normal serum IgG, IgA, and IgM levels but high IgE (44,226 IU/mL); protective protein antigen IgG responses; and IgM responses to isohemagglutinins. He had increased $CD3^+$ and $CD3^+CD4^+$ T-cell counts with a predominance of effector memory $CD4^+$ T cells in the flow cytometric analysis (Table I). T-cell proliferation with anti-CD3/anti-CD28 antibodies and PHA as week as upregulation of CD25 and CD69 were normal in the patient when compared with the healthy controls (see Fig E2 in this article's Online Repository at www.jacionline.org).

### Identification of pathogenic STAT6 variant

WES analysis revealed a novel heterozygous G>A substitution in exon 22 of *STAT6* (c.1114G>A, p.E372K; based on STAT6 isoform 1, NM_003153.5) (Table E1). This mutation, which mapped to the DNA binding domain of STAT6 and was confirmed by Sanger sequencing, has not been previously reported in the genomAD, ExAC, dbSNP, or 1000 Genomes Project databases, and it involved an amino acid residue that is conserved among species (Fig 1, *B-D*). Interestingly, this variant was previously identified in the COSMIC (Catalog of Somatic Mutations in Cancer) database as a somatic mutation associated with lymphoid malignancies.[47] It was not detected in DNA sequences of other available family members, including the mother and siblings, suggesting that it was sporadic. The deleteriousness of the variant was suggested by a high CADD (Combined Annotation Dependent Depletion) score of 27.9. The *in silico* pathogenicity scores of SIFT (Sorting Intolerant From Tolerant), REVEL (Rare Exome Variant Ensemble Learner), Mutation tester, and PROVEAN (Protein Variation Effect Analyzer) were also damaging. The mutation was predicted to minimally affect protein stability as evaluated *in silico* by PremPS (Predicting the Impact of Missense Mutations on Protein Stability) (see Fig E3, *A* in this article's Online Repository at www.jacionline.org).[48] Multiple sequence alignment analysis of STAT6 with other STAT proteins produced by ClusterW and ESpript (https://espript.ibcp.fr/ESPript/ESPript/) showed that the $STAT6^{E372K}$ variant is homologous to $STAT3^{N420K}$, which has been reported as GOF in the literature (Fig E3, *B*).[49,50] Similar to $STAT3^{N420K}$, $STAT6^{E372K}$ features an elongated side chain compared with that of WT (Fig 1, *E* and *F*). Such an extension increases the possibility of additional protein-DNA contact. Moreover, change of the side charge from neutral ($STAT3^{N420K}$) or negative ($STAT6^{E372K}$) to positive is likely to enable the interactions to the negatively charged DNA

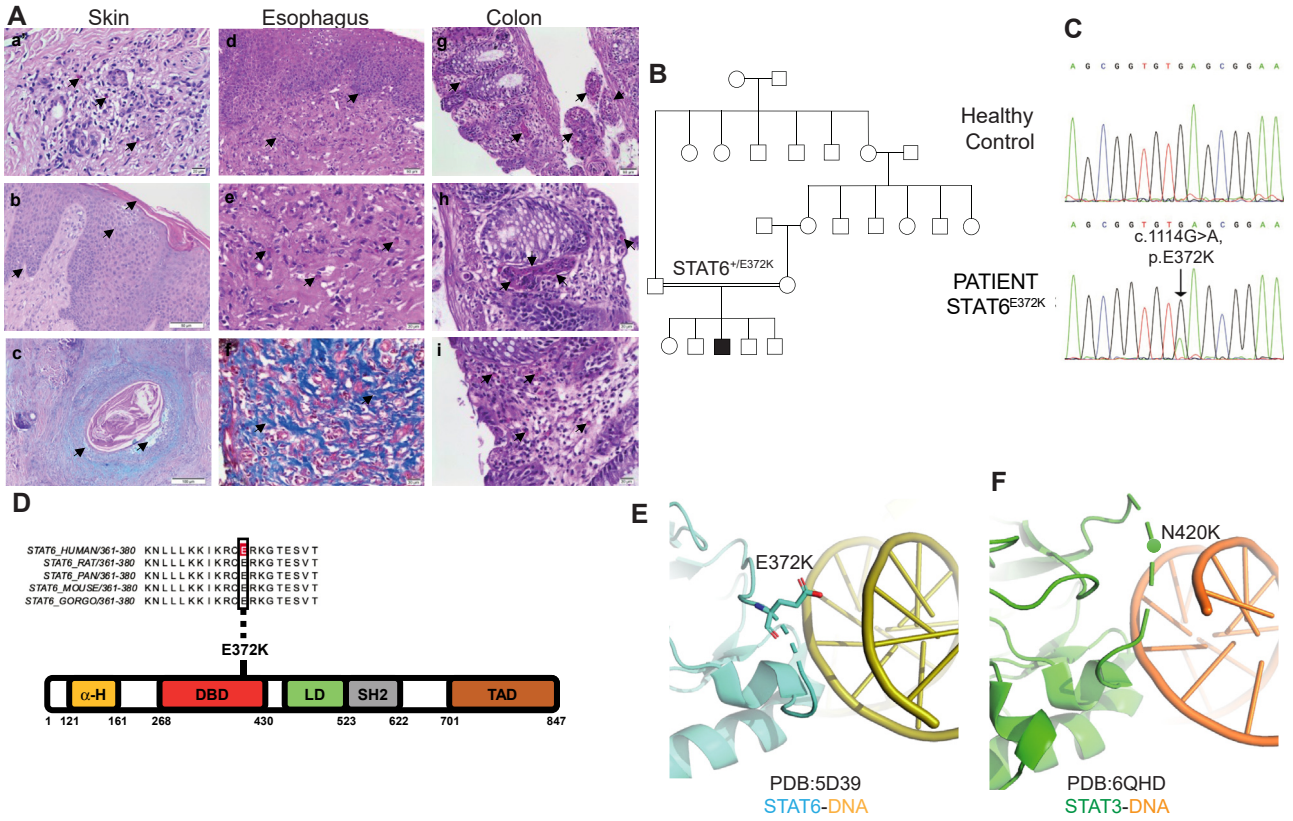


**FIG 1.** Identification of a STAT6$^{E372K}$ mutation in a child with severe allergy dysregulation. **(A)** Scattered eosinophils in dermis; hematoxylin and eosin staining (*H&E*), original magnification 40× **(a)**. Parakeratosis, spongiosis, and acanthosis of epidermis (*black arrows*); H&E, original magnification 20× **(b)**. Mucin accumulation dissociating epithelial cells of follicular epithelium, dilatation of follicle (*black arrows*); periodic acid–Schiff and Alcian blue 2.5 staining, original magnification 10× **(c)**. Gastrointestinal pathology shows esophagitis and scattered eosinophils with marked fibrosis in the subepithelial area of the esophagus (*black arrows*); H&E, original magnification 20× **(d)** and 40× **(e)**; trichrome staining, original magnification 40× **(f)**. Inflammation with eosinophils in lamina propria, intraepithelial, and intravascular areas of sigmoid colon; H&E, original magnification 20× **(g)**, 40× **(h)**, and 40× **(i)**. **(B)** Pedigree of patient with STAT6 GOF. *Double lines* indicate consanguinity; a *filled black square* depicts the patient. Males and females are distinguished by *squares* and *circles*, respectively. **(C)** Sanger sequencing analysis of the *STAT6* c.1114G>A mutation in the index patient versus a healthy control. **(D)** Schematic diagram of STAT6 protein domains. The depicted domains are the α-Helix domain (*α-H*), DNA binding domain (*DBD*), linker domain (*LD*), SH2 domain (*SH2*), and a transactivation domain (*TAD*). The heterozygous mutation localizes to the DBD. Multiple sequence alignment analysis of STAT6 proteins of different species demonstrates conservation of the STAT6$^{E372}$ residue. **(E** and **F)** Structural modeling of the interaction of the STAT6$^{E372K}$ and STAT3$^{N420K}$ with DNA.

phosphate groups. Overall, these analyses suggested that the STAT6$^{E372K}$ variant is deleterious and may act as GOF mutation.

## The STAT6$^{E372K}$ mutation is associated with dysregulated $T_H2$-cell responses

Based on the role of STAT6 in $T_H2$-cell responses, we analyzed circulating CD4$^+$ T-cell subtypes including naive, memory, $T_H1$, $T_H2$, $T_H17$, Treg, and circulating follicular helper T ($cT_{FH}$) cells. The gating strategy is presented in Fig E4 in this article's Online Repository (available at www.jacionline.org). The patient with the STAT6$^{E372K}$ variant exhibited an increased frequency of circulating memory CD4$^+$ T cells (CD3$^+$CD4$^+$CD45RA$^-$CD45RO$^+$) and a decreased frequency of circulating naive CD4$^+$ T cells (CD3$^+$CD4$^+$CD45RA$^+$CD45RO$^-$) (Fig 2, *A*). More detailed analysis of the CD4$^+$ T-cell compartment revealed that the patient with the STAT6$^{E372K}$ variant had an increase of $T_H2$ CD4$^+$ T cells as reflected by the expression of the $T_H2$-cell markers GATA3, CRTH2 (chemoattractant receptor homologous molecule expressed on $T_H2$-type cells), and CCR4 (CD3$^+$CD4$^+$GATA3$^+$, CD3$^+$CD4$^+$CRTH2$^+$, and CD3$^+$CD4$^+$CCR4$^+$). There was also a trend toward decreased expression of $T_H1$- (CD3$^+$CD4$^+$CXCR3$^+$) and $T_H17$- (CD3$^+$CD4$^+$RORγT, CD3$^+$CD4$^+$CCR6$^+$) cell markers (Fig 2, *B* and *C*). Treg-cell analysis also revealed an increase of $T_H2$-skewed Treg cells,[31] indicative of their $T_H2$-cell-like reprogramming (CD3$^+$CD4$^+$CD127$^-$Foxp3$^+$GATA3$^+$, CD3$^+$CD4$^+$CD127$^-$Foxp3$^+$CRTH2$^+$, and CD3$^+$CD4$^+$CD127$^-$Foxp3$^+$CCR4$^+$) and a decrease of $T_H1$ (CD3$^+$CD4$^+$CD127$^-$Foxp3$^+$CXCR3$^+$) and $T_H17$ (CD3$^+$CD4$^+$CD127$^-$Foxp3$^+$RORγt$^+$, CD3$^+$CD4$^+$CD127$^-$Foxp3$^+$CCR6$^+$) Treg cells (Fig 2, *D* and *E*). Further analysis also revealed a decrease of $cT_{FH}$ (CD4$^+$CXCR5$^+$PD1$^+$) cells, skewing these cells toward a $T_H2$ phenotype (CD4$^+$CXCR5$^+$CD45RA$^-$CXCR3$^-$CCR6$^-$) and away from other $T_{FH}$-cell phenotypes including

**TABLE I.** Immunologic evaluation of the patient with STAT6$^{E372K}$ GOF mutation

| Parameters | Before ruxolitinib | | | On ruxolitinib | Normal range for age |
|---|---|---|---|---|---|
| Age (y) | 8 | 9 | 10 | 10 | |
| Complete blood count | | | | | |
| Lymphocyte, n/mm$^3$ | 5,100 | 2,700 | 1,800 | 3,660 | 1,500-8,500 |
| Neutrophil, n/mm$^3$ | 9,600* | 4,900 | 4,800 | 2,600 | 1,500-6,500 |
| Eosinophil, /mm$^3$ | 3,100* | 2,130* | 1,140* | 440 | 0-500 |
| Hemoglobin, g/dL | 9.5* | 10.6 | 8.6* | 11.4 | 10-15.5 |
| Thrombocyte, n/mm$^3$ | 831,000* | 633,000* | 167,000 | 492,000 | 150,000-450,000 |
| Immunoglobulins and antibody responses | | | | | |
| IgG, mg/dL | 1,610 | 1,391 | 1,803 | 1,410 | 842-1,953 |
| IgA, mg/dL | 260 | 152 | 188 | 114 | 62-398 |
| IgM, mg/dL | 116 | 178 | 173 | 109 | 54-392 |
| IgE, IU/mL | 44,626* | 50,000* | 39,700* | 37,550* | <50 |
| Anti-Hbs, mIU/mL | 154 | On IVIG | On IVIG | On IVIG | >10 |
| Anti-mumps (ındex) | 1.53 | On IVIG | On IVIG | On IVIG | >1.1 |
| Isohemagglutinin titer (anti A-IgM) | 1/256 | On IVIG | On IVIG | On IVIG | ≥1/8 |
| Isohemagglutinin titer (anti B-IgM) | 1/64 | On IVIG | On IVIG | On IVIG | ≥1/8 |
| Lymphocyte subsets, n/mm$^3$ | | | | | |
| CD3$^+$ T cells | 4,539* | 2,268 | 1,585 | 3,100 | 1,214-4,130 |
| CD3$^+$4$^+$ T cells | 3,162* | 1,674 | 1,200 | 2,340 | 607-2,110 |
| CD3$^+$8$^+$ T cells | 1,224 | 540 | 325 | 640 | 380-2,084 |
| CD19$^+$ B cells | 255 | 120* | 80* | 296 | 197-867 |
| CD16$^+$56$^+$ NK cells | 255 | 126 | 90 | 114 | 111-963 |
| CD4$^+$ T-cell subsets, % | | | | | |
| CD4$^+$CD45RA$^+$CCR7$^+$ | 61 | NA | 51 | 72 | 40-78 |
| CD4$^+$CD45RA$^-$CCR7$^+$ | 11* | NA | 12* | 9* | 17-53 |
| CD4$^+$CD45RA$^-$CCR7$^-$ | 22* | NA | 30* | 14 | 2-14 |
| CD4$^+$CD45RA$^+$CCR7$^-$ | 5 | NA | 6 | 6 | 0-43 |
| CD8$^+$ T-cell subsets, % | | | | | |
| CD8$^+$CD45RA$^+$CCR7$^+$ | 46 | NA | 53 | 77 | 22-67 |
| CD8$^+$CD45RA$^-$CCR7$^+$ | 3 | NA | 3 | 7 | 1-10 |
| CD8$^+$CD45RA$^-$CCR7$^-$ | 28 | NA | 25 | 9 | 6-41 |
| CD8$^+$CD45RA$^+$CCR7$^-$ | 22 | NA | 18 | 6 | 18-74 |
| CD19 cell subsets (%) | | | | | |
| CD19$^+$CD27$^-$IgD$^+$ | 69 | NA | 50 | 71 | 55-90 |
| CD19$^+$CD27$^+$IgD$^+$ | 6* | NA | 7 | 7 | 7-31 |
| CD19$^+$CD27$^+$IgD$^-$ | 18 | NA | 25 | 12 | 2-52 |
| CD21$^{low}$CD3$^{low}$ B cells | 11 | NA | 3 | 12 | 1-13 |
| IgRT (mg/kg/3 wk) | — | 400 | 400 | 400 | |
| Antibacterial prophylaxis | — | TMP-SMX | TMP-SMX | TMP-SMX | |
| Antifungal prophylaxis | — | — | Fluconazole | — | |
| Antiviral prophylaxis | — | — | — | Aciclovir | |

The following immune cell populations were defined by the respective cell markers: CD4$^+$ naive T cells (CD4$^+$CD45RA$^+$CCR7$^+$), central memory CD4$^+$ T cells (CD4$^+$CD45RA$^-$CCR7$^+$), effector memory CD4$^+$ T cells (CD4$^+$CD45RA$^-$CCR7$^-$), terminally differentiated effector memory CD4$^+$ T cells (CD4$^+$CD45RA$^+$CCR7$^-$), CD8$^+$ naive T cells (CD8$^+$CD45RA$^+$CCR7$^+$), central memory CD8$^+$ T cells (CD8$^+$CD45RA$^-$CCR7$^+$), effector memory CD8$^+$ T cells (CD8$^+$CD45RA$^-$CCR7$^-$), terminally differentiated effector memory CD8$^+$ T cells (CD8$^+$CD45RA$^+$CCR7$^-$), naive mature B cells (CD19$^+$CD27$^-$IgD$^+$), nonswitched memory B cells (CD19$^+$CD27$^+$IgD$^+$), switched memory B cells (CD19$^+$CD27$^+$IgD$^-$), autoreactive B cells (CD21$^{low}$CD3$^{low}$).

*Anti-Hbs,* Anti-hepatitis B surface antibody; *IgRT*, immunoglobulin replacement therapy; *NA*, not available; *NK*, natural killer; *TMP-SMX*, trimethoprim-sulfamethoxazole.

*Abnormal values.

$T_{FH}$1-like (CD4$^+$CXCR5$^+$CD45RA$^-$CXCR3$^+$CCR6$^-$) and $T_{FH}$17-like (CD4$^+$CXCR5$^+$CD45RA$^-$CXCR3$^-$CCR6$^+$) (Fig 2, *F*). There was also an increase in circulating follicular Treg cells (CD4$^+$CXCR5$^+$PD1$^+$CD127$^-$Foxp3$^+$) (Fig 2, *F*).

## The STAT6$^{E372K}$ mutation is associated with enhanced B-cell switching to IgE

Analysis of patient peripheral blood B cells revealed a similar frequency of CD19$^+$CD27$^+$IgD$^-$ class-switched memory B cells but increased frequency of circulating CD19$^+$CD20$^-$CD38$^+$ plasmablasts relative to control subjects (Fig 3, *A-C*). In particular, there was a high frequency of circulating CD19$^+$CD27$^+$IgE$^+$ B cells in the patient relative to controls (Fig 3, *D*). This increase reflected in part heightened expression on circulating patient B cells of the IL-4–inducible low-affinity IgE receptor (CD23) (Fig 3, *E*),[51] which could then bind circulating IgE regardless of the status of the B-cell class-switch isotype. Further analysis revealed that a subset of circulating B cells that do not express CD23 still exhibited IgE staining, raising the possibility of enhanced switching to IgE (Fig 3, *F*).

To determine the propensity of patient B cells to switch to IgE, we sorted naive B cells (CD19$^+$IgD$^+$CD27$^-$CD23$^-$IgE$^-$) to high purity (≥97%) following a gating strategy outlined in Fig 4,

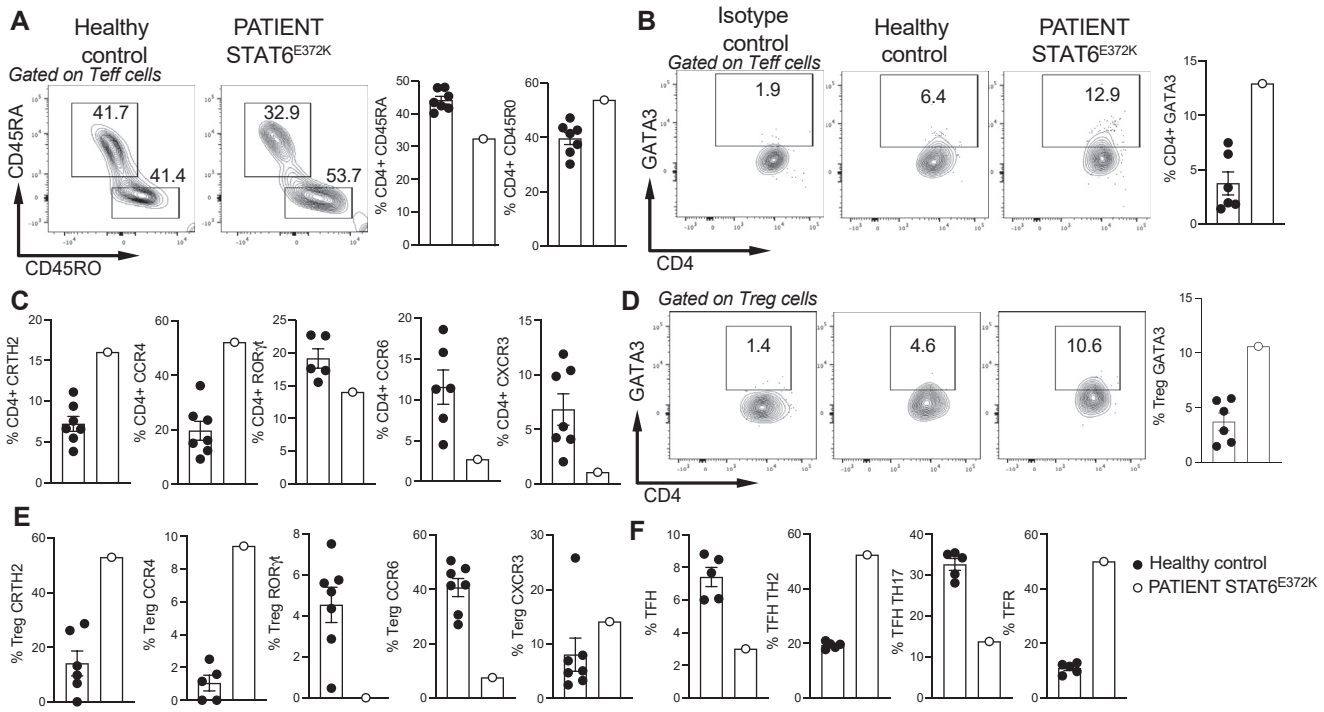


**FIG 2.** The STAT6$^{E372K}$ mutation is associated with skewed $T_H2$-cell responses. **(A)** Flow cytometric analysis and graphical representation of naive ($CD3^+CD4^+CD45RO^-CD45RA^+$) and memory ($CD3^+CD4^+CD45RO^+CD45RA^-$) effector T (Teff) cells in healthy controls and the patient with STAT6$^{E372K}$ mutation. **(B)** Flow cytometric analysis and graphical representation of $T_H2$ cells ($CD3^+CD4^+GATA3^+$) in the respective groups. **(C)** Cells frequencies of $CD4^+CRTH2^+$, $CD4^+CCR4^+$, $CD4^+ROR\gamma^+$, $CD4^+CCR6^+$, and $CD4^+CXCR3^+$ T cells in the respective groups. **(D)** Flow cytometric analysis and graphical representation of Treg $GATA3^+$ cells ($CD3^+CD4^+CD127^-Foxp3^+GATA3^+$) in the respective groups. **(E)** Cells frequencies of Treg $CRTH2^+$, Treg $CCR4^+$, Treg $ROR\gamma T^+$, Treg $CCR6^+$, and Treg $CXCR3^+$ T cells in the respective groups. **(F)** Cells frequencies of $cT_{FH}$, $T_{FH}$ $T_H2$ ($CD4^+CXCR5^+CD45RA^-CXCR3^-CCR6^-$), $T_{FH}T_H17$ ($CD4^+CXCR5^+CD45RA^-CXCR3^-CCR6^+$), and T follicular regulatory ($T_{FR}$) cells in the respective groups. Each symbol represents one subject. Numbers in flow plots indicate percentages. Error bars indicate SEM.

*A* and *B*. The cells were cultured *in vitro* and stimulated with anti-CD40 mAb+IL-4 to induce switching to IgE.[52] Results showed that the patient B cells exhibited markedly increased IgE staining and total IgE in the supernatants at the end of the culture, which is indicative of enhanced switching to IgE (Fig 4, *C* and *D*)

## STAT6$^{E372K}$ is a GOF mutation

Analysis of primary $CD4^+$ T cells revealed a modest increase in the expression of STAT6 in the patient relative to the controls (Fig 5, *A*). To further characterize the functional significance of this mutation, primary T cells were stimulated with IL-4 for 5-30 minutes, and analysis by phosphoflow revealed that the STAT6$^{E372K}$ mutation induces hyperphosphorylation of STAT6, which was evidenced at baseline and increased dramatically post–IL-4 stimulation (Fig 5, *B*). Stimulation with IL-2 or IL-6 resulted in similar levels of STAT5 and STAT3 phosphorylation, respectively, in patient and control T cells (Fig 5, *C*). The STAT6$^{E372K}$ mutation did not appear to delay the STAT6 dephosphorylation on cytokine deprivation as evidenced by a rapid p-STAT6 decline, indicating that its main effect is to enhance the phosphorylation of STAT6 by the JAKs (Fig 3, *D*).

To further assess the impact of this mutation on STAT6 activity, we transfected HEK293 cells with either STAT6$^{E372K}$ or control STAT6$^{WT}$ expression plasmids and analyzed STAT6 protein expression and p-STAT6 formation in response to IL-4 treatment. Flow cytometric analysis revealed that the STAT6$^{E372K}$ mutation did not impact STAT6 protein expression in HEK293 (Fig 5, *E*). To analyze the role of this mutation on the STAT6 activation, phosphoflow analysis revealed that treatment of the respectively transfected cells with IL-4 resulted in increased phosphorylation of the STAT6$^{E372K}$ mutant compared to STAT6$^{WT}$ (Fig 5, *F*). This increase persisted when the phosphoflow staining was normalized for STAT6 expression. We further analyzed the capacity of the STAT6$^{E372K}$ mutant to upregulate STAT6-dependent gene expression compared to STAT6$^{WT}$ by cotransfecting HEK293 cells with a luciferase gene driven by STAT6 response elements together with the respective STAT6 expressing construct. Results showed that the STAT6$^{E372K}$ mutant drove higher expression of the luciferase gene early (1 hour) compared to STAT6$^{WT}$, but that this increase was tempered at later time points (Fig 5, *G*). We also analyzed the nuclear translocation of p-STAT6 species in HEK293 cells that were transfected with either STAT6$^{WT}$ or the STAT6$^{E372K}$ mutant and then stimulated with IL-4. The p-STAT6$^{E372K}$ mutant exhibited a modest increase in nuclear translocation at baseline relative to p-STAT6$^{WT}$. IL-4 treatment

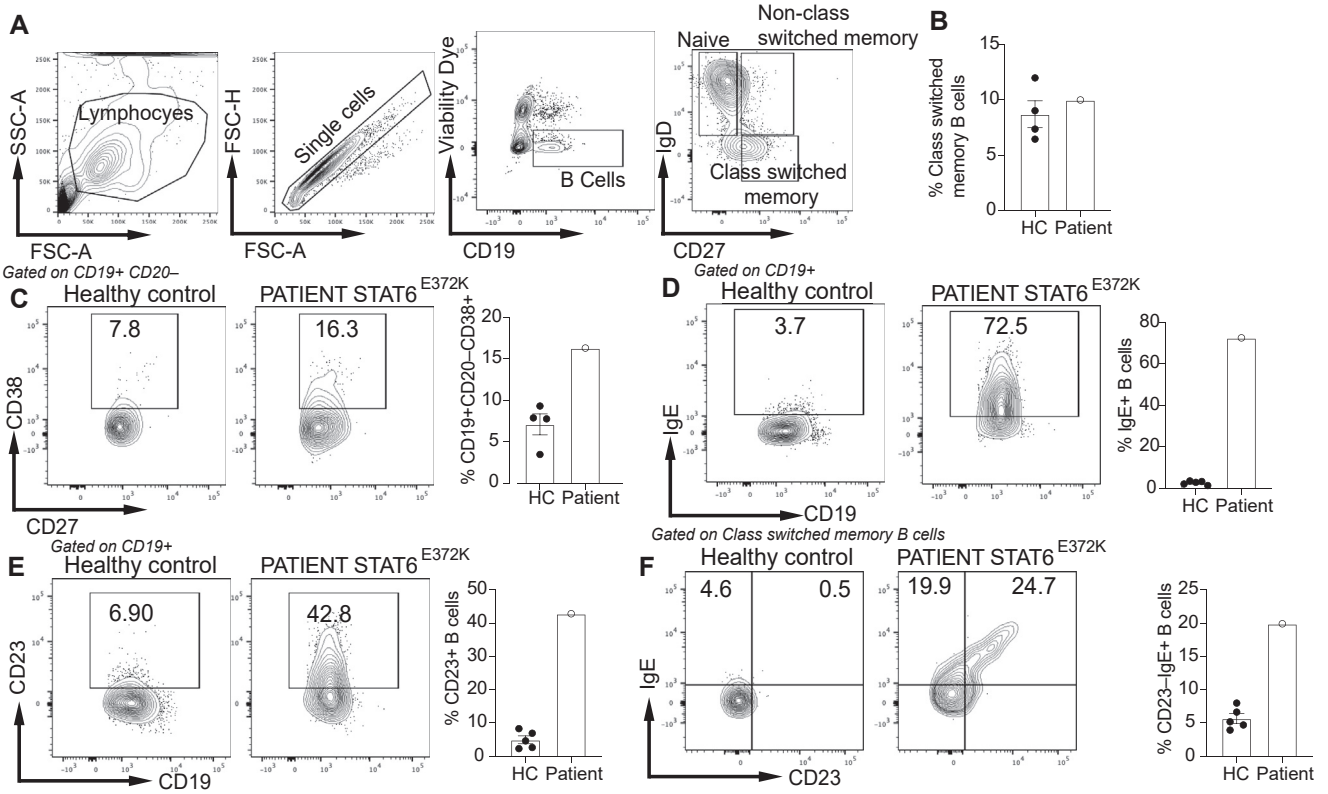


**FIG 3.** The STAT6$^{E372K}$ mutation is associated with increased circulating CD23$^+$ and IgE$^+$ memory B cells. **(A)** Gating strategy for B-cell analysis. **(B)** Cell frequencies of class-switched memory B cells (CD19$^+$, CD27$^+$ IgD$^-$). **(C)** Flow cytometric analysis and graphical representation of plasmablasts (CD19$^+$ CD20$^-$ CD38$^+$) in healthy controls (*HC*) and in the patient with STAT6$^{E372K}$ mutation. **(D)** Flow cytometric analysis and graphical representation of IgE$^+$ circulating B cells in healthy controls and in the patient with the STAT6$^{E372K}$ mutation. **(E** and **F)** Flow cytometric analysis and graphical representation of CD23$^+$ **(E)** and CD23–IgE$^+$ memory (IgD$^-$CD27$^+$) B cells **(F)** in healthy controls and in the patient with STAT6$^{E372K}$ mutation. Each symbol represents one subject. Numbers in flow plots indicate percentages. Error bars indicate SEM. *A*, Area; *FSC*, forward scatter area; *H*, height; *SSC*, side scatter.

resulted in progressive nuclear translocation of p-STAT6 over the 4-hour duration of the study that was markedly increased for p-STAT6$^{E372K}$ mutant relative to p-STAT6$^{WT}$ (Fig 5, *H* and *I*). Overall, these results demonstrated that the STAT6$^{E372K}$ is a GOF mutation that upregulates phosphorylation and the nuclear translocation of STAT6.

## Ruxolitinib therapy suppresses the allergic dysregulation caused by STAT6$^{E372K}$

Based on the immunologic studies showing STAT6$^{E372K}$ as a GOF mutation, and in view of the success of Jakinib therapy in patients with STAT GOF mutations, we initiated therapy of our patient with oral ruxolitinib (10 mg/m$^2$/dose, twice daily). Ruxolitinib rapidly controlled the skin disease with decreased itching noticed within 3 days of therapy. The SCORAD levels decreased from 96 to 25, and ruxolitinib therapy induced almost normal skin hydration and appearance at 1 month post therapy (Fig 6, *A*). A normalization in blood eosinophil number and decrease in serum IgE levels were noticed (Table I). Ruxolitinib therapy was not associated with drug-related adverse effects or infections. Currently, he continues to do well after 6 months of therapy with a most recent SCORAD of 8. Furthermore, there was resolution of his eosinophilic esophagitis-associated dysphagia and a catch-up in his weight from 18 kg (below or equal to third percentile) to 24 kg (third percentile).

Immunologic studies carried out at 1 month post initiation of therapy revealed decreased frequencies of circulating memory T cells and an increase in those of naive T cells (Fig 6, *B*). A reduction of the T$_H$2-cell skewing was also noted (Fig 6, *C* and *D*) and was associated with increased T$_H$1- and T$_H$17-cell frequencies (Fig 6, *E* and *F*). The percentage of IL-4–producing circulating CD4$^+$ T cells, which was increased in the patient pre-ruxolitinib, declined on therapy, while those of other T$_H$1- and T$_H$17-cell subsets increased (Fig 6, *G* and *H*). Ruxolitinib treatment did not impact T$_{FH}$-cell frequencies or their T$_H$2-like skewing but normalized the frequencies of circulating Treg and T$_{FR}$ cells (see Fig E5 in this article's Online Repository at www.jacionline.org). Ruxolitinib treatment did not affect the upregulation of activation markers including CD69 and CD25 following *in vitro* T-cell activation nor did it impact T-cell proliferation in response to stimulation with T-cell mitogens including anti-CD3$^+$ anti-CD28 antibodies and PHA (Fig E1). Finally, treatment with ruxolitinib normalized p-STAT6 induction in the patient's T cells both at baseline and in response to cytokine treatment (IL-4) (Fig 6, *I*). These results indicated that treatment with the JAK1

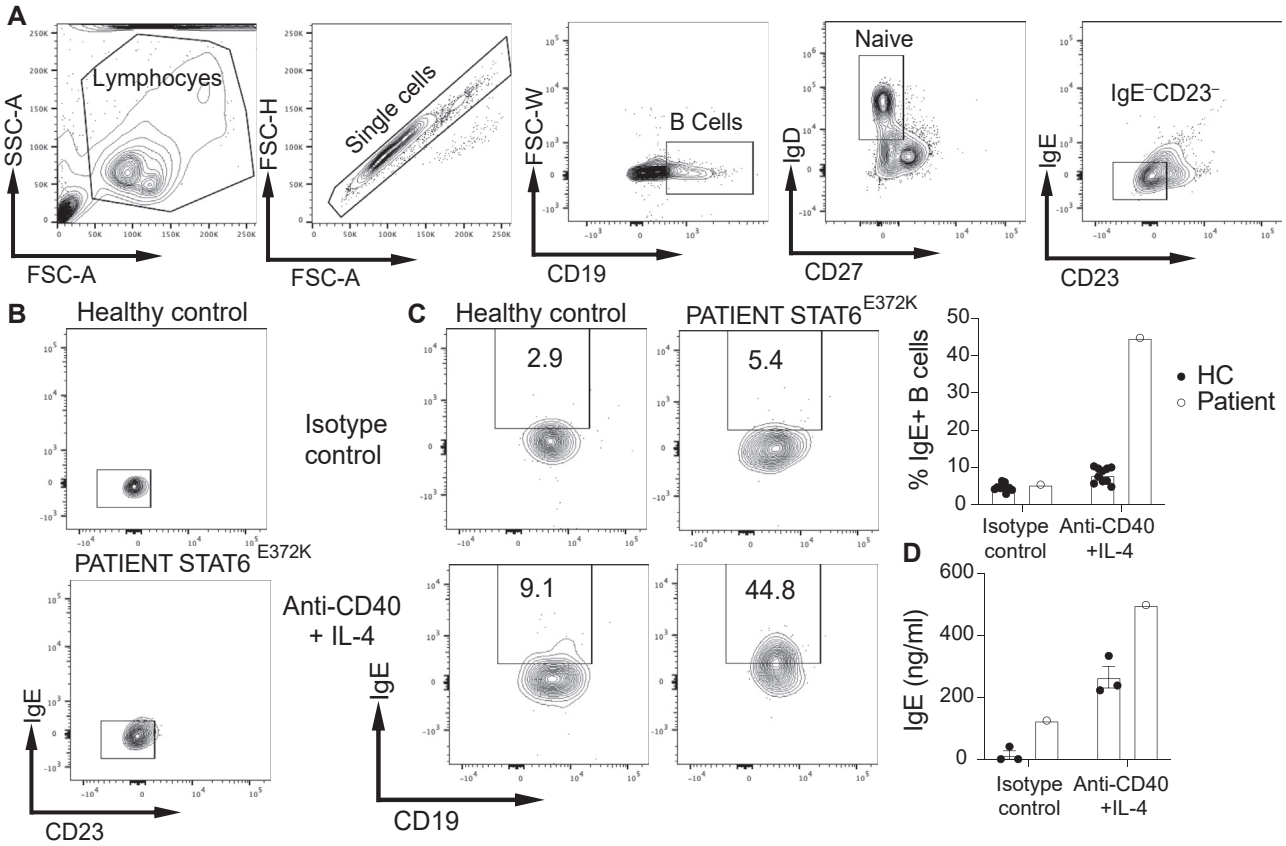


**FIG 4.** The STAT6$^{E372K}$ mutation is associated with enhanced B-cell class switching to IgE. **(A)** Gating strategy for cell-sorting of naive B cells ($CD19^+IgD^+CD27^-CD23^-IgE^-$). **(B)** Purity check after cell sorting. **(C** and **D)** Flow cytometric analysis, frequencies of $IgE^+$ B cells **(C),** and total IgE in the culture supernatants **(D)** in cultures of the respective sorted B-cell populations that were treated with an isotype control mAb or with anti-CD40 mAb+IL-4. Each symbol represents one subject. Numbers in flow plots indicate percentages. Error bars indicate SEM. *W,* Width.

inhibitor ruxolitinib effectively suppressed the clinical and immunologic attributes of the allergic dysregulation associated with STAT6$^{E372K}$ mutation.

## DISCUSSION

In this study, we describe the identification of a STAT6$^{E372K}$ GOF mutation in a child with allergic dysregulation characterized by early onset severe AD accompanied by features mimicking HIES syndrome. The mutation resulted in increased STAT6 activation as evidenced by increased p-STAT6 both at baseline and following IL-4 treatment and accelerated p-STAT6 translocation to the nucleus. STAT6-dependent reporter gene activation was increased early (1 hour) but not later (4 hour) post IL-4 activation, which may reflect increased p-STAT6 sequestration in the nucleus. These alterations in STAT6 activity were associated with enhanced $T_H2$-cell responses and augmented B-cell isotype switching to IgE. Furthermore, the dysregulated STAT6 activity was associated with $T_H2$-cell-like skewing of Treg cells, a phenotype conducive to immune dysregulation and exacerbated allergic inflammation.[31] The capacity of ruxolitinib to suppress the STAT6$^{E372K}$ hyperactivity and ameliorate disease manifestation identify Jakinibs as appropriate targeted therapy in this novel disorder.

STAT6 is a central transcription factor in the nexus of type 2 immunity by virtue of its activation by IL-4 and IL-13 to promote a variety of allergic responses including $T_H2$-cell differentiation,[53] B-cell activation, and IgE production,[22,25] alternate macrophage and epithelial goblet cell differentiation, and innate lymphoid cells type 2 mast cell activation.[54-57] As such, its dysregulation would be predicted to precipitate a broad allergic inflammatory response, as is reflected in the development in our patient of severe AD, eosinophilic esophagitis, food allergy, and hyper-IgE.[58] Some of these phenotypes were reflected in related transgenic mouse models of enhanced STAT6 signaling. The first is an engineered STAT6 mutant with 2 alanine substitutions in the SH2 domain (STAT6VT), whose expression is restricted to lymphoid tissues. The STAT6VT mice develop marked $T_H2$-cell skewing, severe AD-like phenotype with blepharitis and allergic lung inflammation.[36,37] In a second model, an inactivating mutation (IL-4Rα$Y709 \rightarrow F$) was engineered in the immunotyrosine inhibitory motif in the cytoplasmic domain of the IL-4Rα chain, which dampens STAT6 activation by recruiting the phosphotyrosine phosphatase Shp1.[59] Accordingly, the mutant receptor mediated enhanced IL-4– and IL-13–induced STAT6 phosphorylation and activation.[57,59] These mice exhibited augmented allergic responses including allergic airway inflammation and food allergy in part by a mechanism involving the

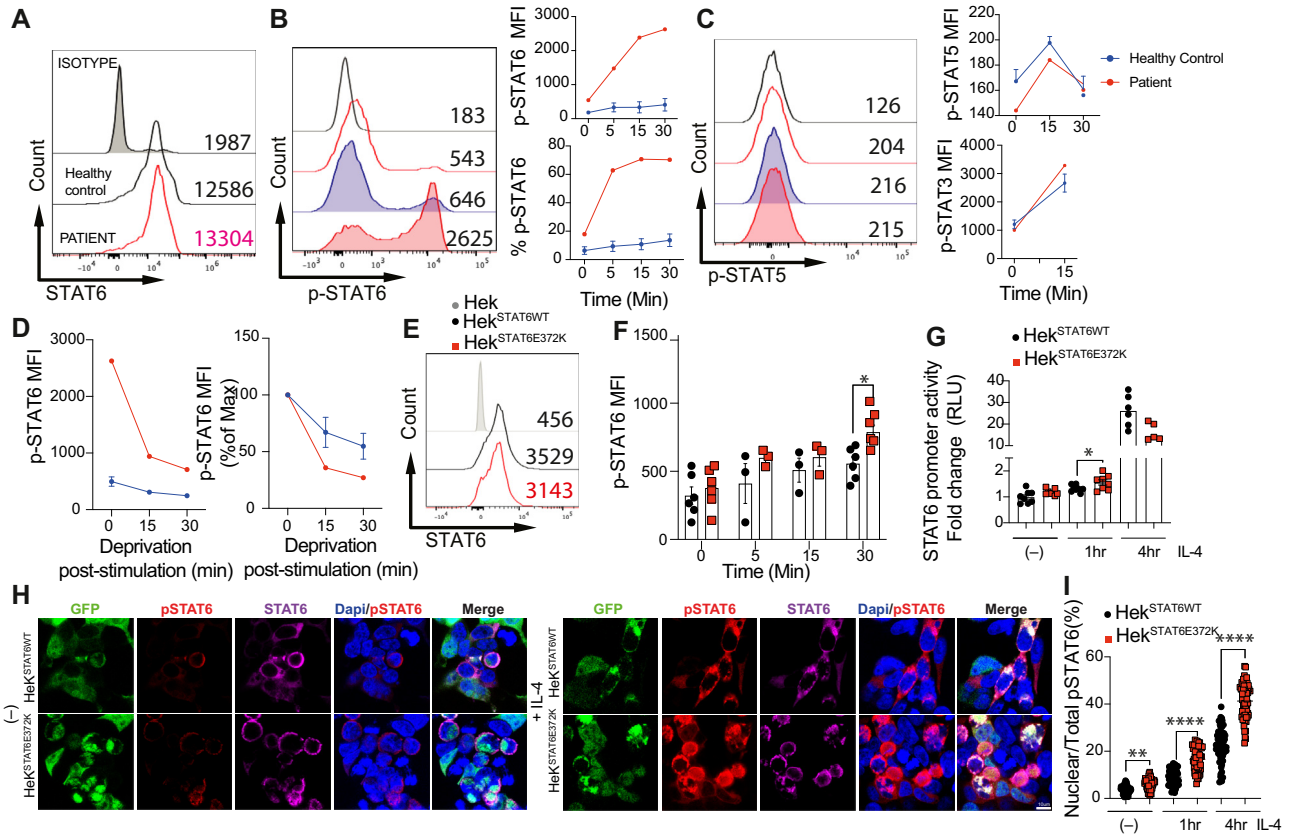


**FIG 5.** $STAT6^{E372K}$ is a GOF mutation. **(A)** Flow cytometric analysis and mean fluorescence intensity (*MFI*) of STAT6 in $CD4^+$ T cells of healthy controls and the patient with $STAT6^{E372K}$ mutation. **(B)** Flow cytometric analysis and MFI of p-STAT6 (*top*) and frequencies of p-STAT6 cells (*bottom*) in $CD4^+$ T cells of healthy controls and the patient with $STAT6^{E372K}$ mutation after stimulation with IL-4 (20 ng/mL) for 5-30 minutes (*black line:* healthy control unstimulated; *red line*: $STAT6^{E372K}$ patient unstimulated; *blue:* healthy control stimulated with IL-4; and *red*: $STAT6^{E372K}$ patient stimulated with IL-4). **(C)** Flow cytometric analysis and MFI of p-STAT5 (*top*) and of p-STAT3 (*bottom*) in $CD4^+$ T cells of healthy controls and the patient with $STAT6^{E372K}$ mutation after stimulation with IL-2 (20 ng/mL) or IL-6 (20 ng/mL), respectively for 5-30 minutes. **(D)** Dephosphorylation kinetics of phospho-STAT6 in response to deprivation of IL-4 and in $CD4^+$ T cells represented as absolute MFI (*left*) and normalized to maximum expression before deprivation (*right*). **(E)** MFI expression of STAT6 in HEK293 cell transfected with either $STAT6^{WT}$ or $STAT6^{E372K}$ proteins. **(F)** MFI expression of p-STAT6 in HEK293 cell transfected with either $STAT6^{WT}$ or $STAT6^{E372K}$ proteins after IL-4 (20 ng/mL) stimulation for 5-30 minutes. **(G)** STAT6 response element-driven luciferase reporter activation by $STAT6^{WT}$ or $STAT6^{E372K}$ transfected into HEK293 cells at baseline and following IL-4 treatment for 1 and 4 hours. **(H and I)** Confocal microscopic analysis of total STAT6, p-STAT6, and 4′-6-diamidino-2-phenylindole, dihydrochloride (*DAPI*) in HEK293 cells transfected with either $STAT6^{WT}$ or $STAT6^{E372K}$ and then either sham-treated or stimulated with IL-4 for 1 and 4 hours, respectively. Numbers in flow plots indicate MFI. Error bars indicate SEM. Statistical tests: $*P < .05$, $**P < .01$, $****P < .0001$ by 2-way ANOVA with Dunnett's post hoc analysis **(F, G, I)**. *RLU*, Relative luciferase unit.

$T_H2$-cell-like reprogramming of their Treg cells, leading to their failure to effectively control allergic responses.[31,60,61] Of note, STAT6VT T effector cells also appear resistant to Treg cell-mediated suppression.[30] Consistent with the $T_H2$-cell-like phenotype of the Treg cells of the patient reported herein, one can postulate that the aberrant $STAT6^{E372K}$ may similarly act in part to impair Treg cell control of the allergic response, giving rise among other things of dysregulated $T_H2$ and $PD1^+$ $T_H2$-like $cT_{FH}$-cell responses to drive the allergic inflammation in our patient.

Somatic GOF mutations in STAT6, including $STAT6^{E372K}$, have been previously described in follicular lymphomas. However, in that report, the E372K mutation was found associated with largely autonomous transcriptional activity independent of IL-4 or STAT6-Y641 phosphorylation.[34] In contrast, our own studies showed that the GOF attributes of the $STAT6^{E372K}$ mutation were overwhelmingly IL-4–dependent in terms of p-STAT6 formation, nuclear translocation, and luciferase reporter activation as well as B-cell switching to IgE. Furthermore, our patient responded to ruxolitinib, which is indicative of IL-4R–driven $STAT6^{E372}$ activation in the patient. These differences may reflect the methods employed in the respective studies.

The identification of a germline GOF mutation in STAT6 expands the spectrum of GOF mutations in JAK-STAT pathways.

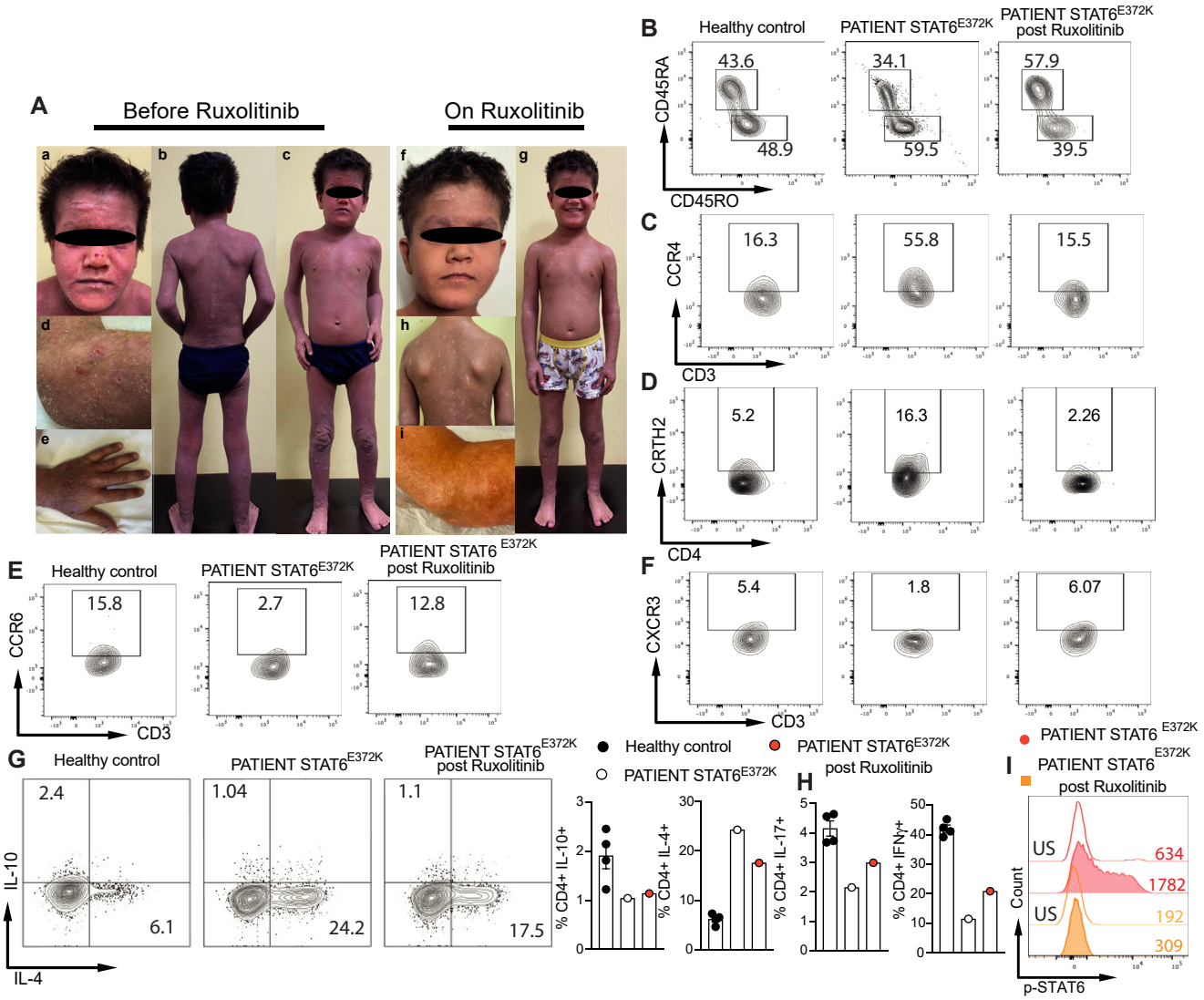


**FIG 6.** Ruxolitinib therapy suppresses the patient's allergic dysregulation and inhibits the $T_H2$-cell skewing and STAT6 hyperactivation. **(A)** Response of patient AD to ruxolitinib therapy. **(a-e)** Severe AD before ruxolitinib therapy covering the face **(a),** body **(b** and **c),** elbow and hand **(d** and **e)** of the patient. **(f-i)** Control of AD after ruxolitinib treatment. **(B)** Flow cytometric analysis of naive ($CD3^+CD4^+CD45RO^-CD45RA^+$) and memory ($CD3^+CD4^+CD45RO^+CD45RA^-$) Teff cells in healthy controls and the patient with $STAT6^{E372K}$ mutation pre- and posttherapy with ruxolitinib. **(C** and **D)** Flow cytometric analysis of $CD4^+CCR4^+$ **(C)** and $CD4^+CRTH2^+$ **(D)** T cells in the respective groups. **(E** and **F)** Cells frequencies of $CD4^+CCR6^+$ **(E)** and $CD4^+CXCR3^+$ **(F)** T cells in the respective groups. **(G** and **H)** Flow cytometric analysis with representative plots of IL-4–, IL-17–, IFN-γ–, and IL-10–producing circulating $CD4^+$ T cells pre- and postruxolitinib therapy compared with healthy controls. **(I)** Flow cytometric analysis and MFI of p-STAT6 (*left*) and p-STAT6 fold change (*right*) in $CD4^+$ T cells of healthy controls and the patient with $STAT6^{E372K}$ mutation pre- and posttreated with ruxolitinib after stimulation with IL-4 (20 ng/mL) for 30 minutes (*red line:* $STAT6^{E372K}$ patient pretreatment unstimulated; *red*: $STAT6^{E372K}$ patient stimulated with IL-4; *orange line*: $STAT6^{E372K}$ patient posttreatment with ruxolitinib; and *orange*: $STAT6^{E372K}$ patient posttreated with ruxolitinib stimulated with IL-4). Each symbol represents one subject. Numbers in flow plots indicate percentages. Error bars indicate SEM.

In these disorders, the Jakinibs are leveraged to control of JAK-STAT pathway and consequently control different disease activities.[62] Recently, data are available on the successful usage of Jakinibs in IEI disorders such as STAT1, STAT3, STAT5B, and JAK1 GOFs; interferonopathies; and SOCS1 haploinsufficiency.[15,42,63-66] We previously showed that treatment with the Jakinib in patients with STAT1 GOF mutations decreased hyperresponsiveness to type I and II interferons, normalized $T_H1$- and $T_{FH}$-cell responses, improved $T_H17$-cell differentiation, cured mucocutaneous candidiasis, and maintained remission of associated autoimmunity.[41,42] The studies herein extend the usage of Jakinibs in primary atopic disorders by establishing disease control in STAT6 GOF disease. However, long-term data regarding the outcome of this targeted therapy are needed to understand the full efficacy of these drugs in controlling the disease symptoms.

Finally, the identification of STAT6 GOF mutations as a cause of severe allergic dysregulation expands our knowledge of the genetic architecture of allergic diseases,[1,12,67-70] and highlights the pivotal role of the IL-4/IL-13/IL4R/STAT6 axis in disease pathogenesis. Establishing the molecular underpinning of these diseases enables the use of targeted therapies to reverse the atopic inflammation and restore immune homeostasis in these patients.[21,71]

We thank Drs Hans Oettgen and Cynthia Kanagaratham for sharing reagents, and Melek Yorgun Altunbas for clinical support.

**Key messages**

- **A germline STAT6 GOF mutation gave rise to severe allergic inflammation.**
- **Therapy with a Jakinib controlled disease manifestations and suppressed the associated immune dysregulation.**

## REFERENCES

1. Nelson RW, Geha RS, McDonald DR. Inborn errors of the immune system associated with atopy. Front Immunol 2022;13:860821.
2. Vaseghi-Shanjani M, Snow AL, Margolis DJ, Latrous M, Milner JD, Turvey SE, et al. Atopy as immune dysregulation: offender genes and targets. J Allergy Clin Immunol Pract 2022;10:1737-56.
3. Holland SM, DeLeo FR, Elloumi HZ, Hsu AP, Uzel G, Brodsky N, et al. STAT3 mutations in the hyper-IgE syndrome. N Engl J Med 2007;357:1608-19.
4. Zhang Q, Davis JC, Lamborn IT, Freeman AF, Jing H, Favreau AJ, et al. Combined immunodeficiency associated with DOCK8 mutations. N Engl J Med 2009;361:2046-55.
5. Engelhardt KR, McGhee S, Winkler S, Sassi A, Woellner C, Lopez-Herrera G, et al. Large deletions and point mutations involving the dedicator of cytokinesis 8 (DOCK8) in the autosomal-recessive form of hyper-IgE syndrome. J Allergy Clin Immunol 2009;124:1289-302.e4.
6. Bergerson JRE, Freeman AF. An update on syndromes with a hyper-IgE phenotype. Immunol Allergy Clin North Am 2019;39:49-61.
7. Bousfiha A, Jeddane L, Picard C, Al-Herz W, Ailal F, Chatila T, et al. Human inborn errors of immunity: 2019 update of the IUIS phenotypical classification. J Clin Immunol 2020;40:66-81.
8. Tangye SG, Al-Herz W, Bousfiha A, Cunningham-Rundles C, Franco JL, Holland SM, et al. Human inborn errors of immunity: 2022 update on the classification from the International Union of Immunological Societies Expert Committee. J Clin Immunol 2022;42:1473-507.
9. Lyons JJ, Milner JD. The clinical and mechanistic intersection of primary atopic disorders and inborn errors of growth and metabolism. Immunol Rev 2019;287:135-44.
10. Al Khatib S, Keles S, Garcia-Lloret M, Karakoc-Aydiner E, Reisli I, Artac H, et al. Defects along the T(H)17 differentiation pathway underlie genetically distinct forms of the hyper IgE syndrome. J Allergy Clin Immunol 2009;124:342-8, 8e1-5.
11. Lyons JJ, Milner JD. Primary atopic disorders. J Exp Med 2018;215:1009-22.
12. Vaseghi-Shanjani M, Smith KL, Sara RJ, Modi BP, Branch A, Sharma M, et al. Inborn errors of immunity manifesting as atopic disorders. J Allergy Clin Immunol 2021;148:1130-9.
13. Milner JD, Vogel TP, Forbes L, Ma CA, Stray-Pedersen A, Niemela JE, et al. Early-onset lymphoproliferation and autoimmunity caused by germline STAT3 gain-of-function mutations. Blood 2015;125:591-9.
14. Kasap N, Aslan K, Karakurt LT, Bozkurt H, Canatan H, Cavkaytar O, et al. A novel gain-of-function mutation in STAT5B is associated with treatment-resistant severe atopic dermatitis. Clin Exp Allergy 2022;52:907-10.
15. Del Bel KL, Ragotte RJ, Saferali A, Lee S, Vercauteren SM, Mostafavi SA, et al. JAK1 gain-of-function causes an autosomal dominant immune dysregulatory and hypereosinophilic syndrome. J Allergy Clin Immunol 2017;139:2016-20.e5.
16. Liu L, Okada S, Kong XF, Kreins AY, Cypowyj S, Abhyankar A, et al. Gain-of-function human STAT1 mutations impair IL-17 immunity and underlie chronic mucocutaneous candidiasis. J Exp Med 2011;208:1635-48.
17. Hou J, Schindler U, Henzel WJ, Ho TC, Brasseur M, McKnight SL. An interleukin-4-induced transcription factor: IL-4 Stat. Science 1994;265:1701-6.
18. Takeda K, Tanaka T, Shi W, Matsumoto M, Minami M, Kashiwamura S, et al. Essential role of Stat6 in IL-4 signalling. Nature 1996;380:627-30.
19. Kaplan MH, Schindler U, Smiley ST, Grusby MJ. Stat6 is required for mediating responses to IL-4 and for development of Th2 cells. Immunity 1996;4:313-9.
20. Nelms K, Keegan AD, Zamorano J, Ryan JJ, Paul WE. The IL-4 receptor: signaling mechanisms and biologic functions. Annu Rev Immunol 1999;17:701-38.
21. Harb H, Chatila TA. Mechanisms of dupilumab. Clin Exp Allergy 2020;50:5-14.
22. Luo Y, Alexander M, Gadina M, O'Shea JJ, Meylan F, Schwartz DM. JAK-STAT signaling in human disease: from genetic syndromes to clinical inhibition. J Allergy Clin Immunol 2021;148:911-25.
23. Levy DE, Darnell JE Jr. Stats: transcriptional control and biological impact. Nat Rev Mol Cell Biol 2002;3:651-62.
24. Schindler C, Darnell JE Jr. Transcriptional responses to polypeptide ligands: the JAK-STAT pathway. Annu Rev Biochem 1995;64:621-51.
25. Wang W, Wang L, Zha B. The roles of STAT6 in regulating B cell fate, activation, and function. Immunol Lett 2021;233:87-91.
26. Palm NW, Rosenstein RK, Medzhitov R. Allergic host defences. Nature 2012;484:465-72.
27. Pulendran B, Artis D. New paradigms in type 2 immunity. Science 2012;337:431-5.
28. Scheinman EJ, Avni O. Transcriptional regulation of GATA3 in T helper cells by the integrated activities of transcription factors downstream of the interleukin-4 receptor and T cell receptor. J Biol Chem 2009;284:3037-48.
29. Maier E, Duschl A, Horejs-Hoeck J. STAT6-dependent and -independent mechanisms in Th2 polarization. Eur J Immunol 2012;42:2827-33.
30. Pillemer BB, Qi Z, Melgert B, Oriss TB, Ray P, Ray A. STAT6 activation confers upon T helper cells resistance to suppression by regulatory T cells. J Immunol 2009;183:155-63.
31. Noval Rivas M, Burton OT, Wise P, Charbonnier LM, Georgiev P, Oettgen HC, et al. Regulatory T cell reprogramming toward a Th2-cell-like lineage impairs oral tolerance and promotes food allergy. Immunity 2015;42:512-23.
32. Hancock DB, Romieu I, Chiu GY, Sienra-Monge JJ, Li H, Estela Del Rio-Navarro B, et al. STAT6 and LRP1 polymorphisms are associated with food allergen sensitization in Mexican children. J Allergy Clin Immunol 2012;129:1673-6.
33. O'Shea JJ, Schwartz DM, Villarino AV, Gadina M, McInnes IB, Laurence A. The JAK-STAT pathway: impact on human disease and therapeutic intervention. Annu Rev Med 2015;66:311-28.
34. Yildiz M, Li H, Bernard D, Amin NA, Ouillette P, Jones S, et al. Activating STAT6 mutations in follicular lymphoma. Blood 2015;125:668-79.
35. von Hoff L, Kargel E, Franke V, McShane E, Schulz-Beiss KW, Patone G, et al. Autocrine LTA signaling drives NF-kappaB and JAK-STAT activity and myeloid gene expression in Hodgkin lymphoma. Blood 2019;133:1489-94.
36. Bruns HA, Schindler U, Kaplan MH. Expression of a constitutively active Stat6 in vivo alters lymphocyte homeostasis with distinct effects in T and B cells. J Immunol 2003;170:3478-87.
37. Sehra S, Bruns HA, Ahyi AN, Nguyen ET, Schmidt NW, Michels EG, et al. IL-4 is a critical determinant in the generation of allergic inflammation initiated by a constitutively active Stat6. J Immunol 2008;180:3551-9.
38. Kolukisa B, Baser D, Akcam B, Danielson J, Bilgic Eltan S, Haliloglu Y, et al. Evolution and long-term outcomes of combined immunodeficiency due to CARMIL2 deficiency. Allergy 2022;77:1004-19.
39. Kiykim A, Ogulur I, Dursun E, Charbonnier LM, Nain E, Cekic S, et al. Abatacept as a long-term targeted therapy for LRBA deficiency. J Allergy Clin Immunol Pract 2019;7:2790-800.e15.
40. Baris S, Alroqi F, Kiykim A, Karakoc-Aydiner E, Ogulur I, Ozen A, et al. Severe early-onset combined immunodeficiency due to heterozygous gain-of-function mutations in STAT1. J Clin Immunol 2016;36:641-8.
41. Kayaoglu B, Kasap N, Yilmaz NS, Charbonnier LM, Geckin B, Akcay A, et al. Stepwise reversal of immune dysregulation due to STAT1 gain-of-function mutation following ruxolitinib bridge therapy and transplantation. J Clin Immunol 2021;41:769-79.
42. Weinacht KG, Charbonnier LM, Alroqi F, Plant A, Qiao Q, Wu H, et al. Ruxolitinib reverses dysregulated T helper cell responses and controls autoimmunity caused by a novel signal transducer and activator of transcription 1 (STAT1) gain-of-function mutation. J Allergy Clin Immunol 2017;139:1629-40.e2.
43. Cui Y, Benamar M, Schmitz-Abe K, Poondi-Krishnan V, Chen Q, Jugder BE, et al. A Stk4-Foxp3-NF-kappaB p65 transcriptional complex promotes T(reg) cell activation and homeostasis. Sci Immunol 2022;7:eabl8357.
44. Schmitz-Abe K, Li Q, Rosen SM, Nori N, Madden JA, Genetti CA, et al. Unique bioinformatic approach and comprehensive reanalysis improve diagnostic yield of clinical exomes. Eur J Hum Genet 2019;27:1398-405.

45. Severity scoring of atopic dermatitis: the SCORAD index. Consensus Report of the European Task Force on Atopic Dermatitis. Dermatology 1993;186:23-31.
46. Grimbacher B, Schaffer AA, Holland SM, Davis J, Gallin JI, Malech HL, et al. Genetic linkage of hyper-IgE syndrome to chromosome 4. Am J Hum Genet 1999;65:735-44.
47. Tate JG, Bamford S, Jubb HC, Sondka Z, Beare DM, Bindal N, et al. COSMIC: the Catalogue Of Somatic Mutations In Cancer. Nucleic Acids Res 2019;47:D941-7.
48. Chen Y, Lu H, Zhang N, Zhu Z, Wang S, Li M. PremPS: Predicting the impact of missense mutations on protein stability. PLoS Comput Biol 2020;16:e1008543.
49. Faletti L, Ehl S, Heeg M. Germline STAT3 gain-of-function mutations in primary immunodeficiency: impact on the cellular and clinical phenotype. Biomed J 2021;44:412-21.
50. Li J, Rodriguez JP, Niu F, Pu M, Wang J, Hung LW, et al. Structural basis for DNA recognition by STAT6. Proc Natl Acad Sci U S A 2016;113:13015-20.
51. Vercelli D, Jabara HH, Lee BW, Woodland N, Geha RS, Leung DY. Human recombinant interleukin 4 induces Fc epsilon R2/CD23 on normal human monocytes. J Exp Med 1988;167:1406-16.
52. Jabara HH, Fu SM, Geha RS, Vercelli D. CD40 and IgE: synergism between anti-CD40 monoclonal antibody and interleukin 4 in the induction of IgE synthesis by highly purified human B cells. J Exp Med 1990;172:1861-4.
53. Elo LL, Jarvenpaa H, Tuomela S, Raghav S, Ahlfors H, Laurila K, et al. Genome-wide profiling of interleukin-4 and STAT6 transcription factor regulation of human Th2 cell programming. Immunity 2010;32:852-62.
54. Van Dyken SJ, Locksley RM. Interleukin-4- and interleukin-13-mediated alternatively activated macrophages: roles in homeostasis and disease. Annu Rev Immunol 2013;31:317-43.
55. Schubart C, Krljanac B, Otte M, Symowski C, Martini E, Gunther C, et al. Selective expression of constitutively activated STAT6 in intestinal epithelial cells promotes differentiation of secretory cells and protection against helminths. Mucosal Immunol 2019;12:413-24.
56. Liang HE, Reinhardt RL, Bando JK, Sullivan BM, Ho IC, Locksley RM. Divergent expression patterns of IL-4 and IL-13 define unique functions in allergic immunity. Nat Immunol 2011;13:58-66.
57. Burton OT, Darling AR, Zhou JS, Noval-Rivas M, Jones TG, Gurish MF, et al. Direct effects of IL-4 on mast cells drive their intestinal expansion and increase susceptibility to anaphylaxis in a murine model of food allergy. Mucosal Immunol 2013;6:740-50.
58. Chapoval S, Dasgupta P, Dorsey NJ, Keegan AD. Regulation of the T helper cell type 2 (Th2)/T regulatory cell (Treg) balance by IL-4 and STAT6. J Leukoc Biol 2010;87:1011-8.
59. Tachdjian R, Al Khatib S, Schwinglshackl A, Kim HS, Chen A, Blasioli J, et al. In vivo regulation of the allergic response by the IL-4 receptor alpha chain immunoreceptor tyrosine-based inhibitory motif. J Allergy Clin Immunol 2010;125:1128-36.e8.
60. Massoud AH, Charbonnier LM, Lopez D, Pellegrini M, Phipatanakul W, Chatila TA. An asthma-associated IL4R variant exacerbates airway inflammation by promoting conversion of regulatory T cells to TH17-like cells. Nat Med 2016;22:1013-22.
61. Noval Rivas M, Burton OT, Oettgen HC, Chatila T. IL-4 production by group 2 innate lymphoid cells promotes food allergy by blocking regulatory T-cell function. J Allergy Clin Immunol 2016;138:801-11.e9.
62. Gadina M, Johnson C, Schwartz D, Bonelli M, Hasni S, Kanno Y, et al. Translational and clinical advances in JAK-STAT biology: the present and future of Jakinibs. J Leukoc Biol 2018;104:499-514.
63. Forbes LR, Vogel TP, Cooper MA, Castro-Wagner J, Schussler E, Weinacht KG, et al. Jakinibs for the treatment of immune dysregulation in patients with gain-of-function signal transducer and activator of transcription 1 (STAT1) or STAT3 mutations. J Allergy Clin Immunol 2018;142:1665-9.
64. Balci S, Ekinci RMK, de Jesus AA, Goldbach-Mansky R, Yilmaz M. Baricitinib experience on STING-associated vasculopathy with onset in infancy: a representative case from Turkey. Clin Immunol 2020;212:108273.
65. Hadjadj J, Castro CN, Tusseau M, Stolzenberg MC, Mazerolles F, Aladjidi N, et al. Early-onset autoimmunity associated with SOCS1 haploinsufficiency. Nat Commun 2020;11:5341.
66. Eisenberg R, Gans MD, Leahy TR, Gothe F, Perry C, Raffeld M, et al. JAK inhibition in early-onset somatic, nonclonal STAT5B gain-of-function disease. J Allergy Clin Immunol Pract 2021;9:1008-10.e2.
67. Vercelli D. Discovering susceptibility genes for asthma and allergy. Nat Rev Immunol 2008;8:169-82.
68. Milner JD. Primary atopic disorders. Annu Rev Immunol 2020;38:785-808.
69. Gupta J, Johansson E, Bernstein JA, Chakraborty R, Khurana Hershey GK, Rothenberg ME, et al. Resolving the etiology of atopic disorders by using genetic analysis of racial ancestry. J Allergy Clin Immunol 2016;138:676-99.
70. SoRelle JA, Chen Z, Wang J, Yue T, Choi JH, Wang KW, et al. Dominant atopy risk mutations identified by mouse forward genetic analysis. Allergy 2021;76:1095-108.
71. Shankar A, McAlees JW, Lewkowich IP. Modulation of IL-4/IL-13 cytokine signaling in the context of allergic disease. J Allergy Clin Immunol 2022;150:266-76.


**FIG E1.** Joint hyperextensibility and dental abnormalities in the patient with STAT6 GOF disease. **(A)** Hyperextensibility in the patient according to the Beighton score screening technique for hypermobility. **(B)** Enamel hypoplasia (*white arrows*) and normal dentition without delay shedding in decidual teeth.

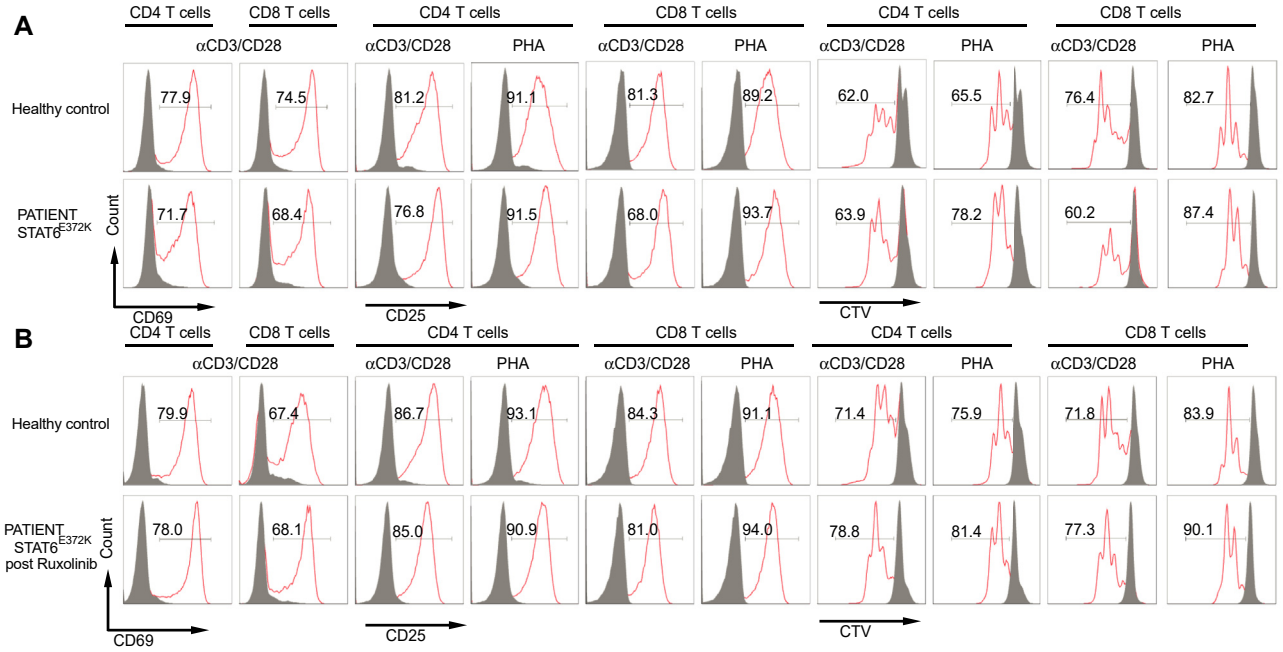


**FIG E2.** T-cell activation and proliferation in STAT6 GOF disease. **(A** and **B)** Flow cytometric analysis of anti-CD3+anti-CD28 antibody-stimulated healthy control subject and patient PBMCs obtained in the patient pre- **(A)** and post- **(B)** ruxolitinib therapy and analyzed for CD69 (at 24 hours poststimulation) and CD25 and CellTrace Violet (*CTV*) (at 72 hours poststimulation). *Gray histograms* represent staining with isotype control antibodies.

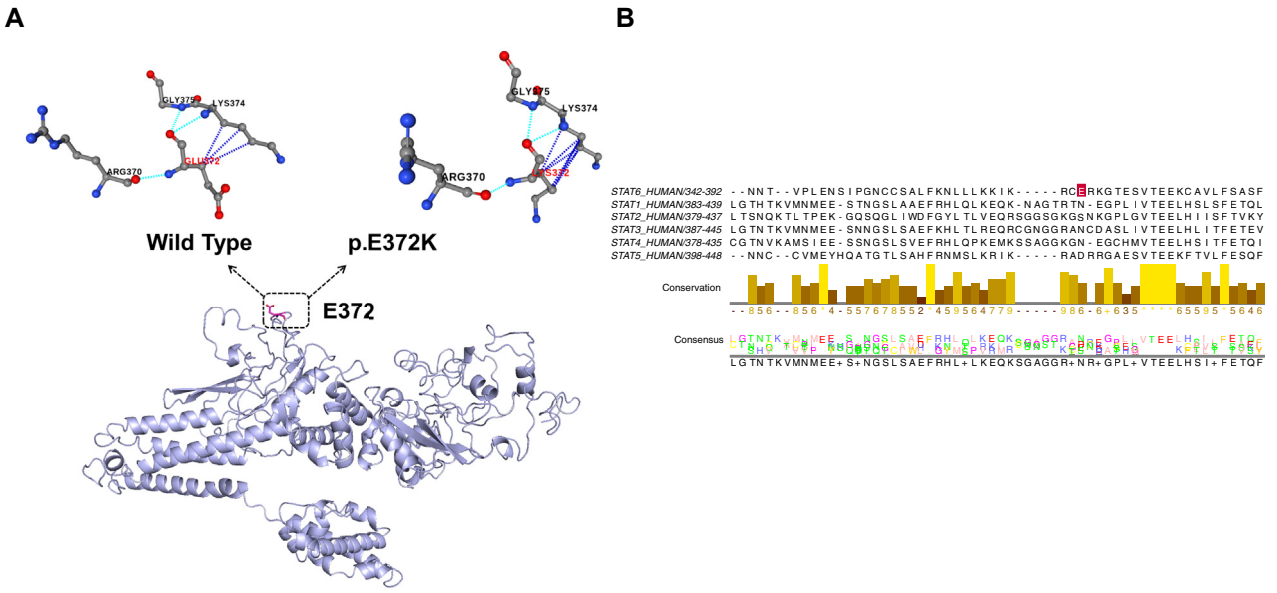


**FIG E3.** Structural analysis of the STAT6$^{E372K}$ variant. **(A)** Impact of the STAT6$^{E372K}$ mutation on protein stability as evaluated by PremPS. Hydrophobic interactions (*top right*) appeared compared to WT (*top left*), without causing any change in interacting residues or other bonds. **(B)** Sequence alignment of STAT6 and other STAT proteins produced by ClusterW and ESpript. The location of STAT6$^{E372}$ and homologous residues in the respective STAT proteins is indicated.

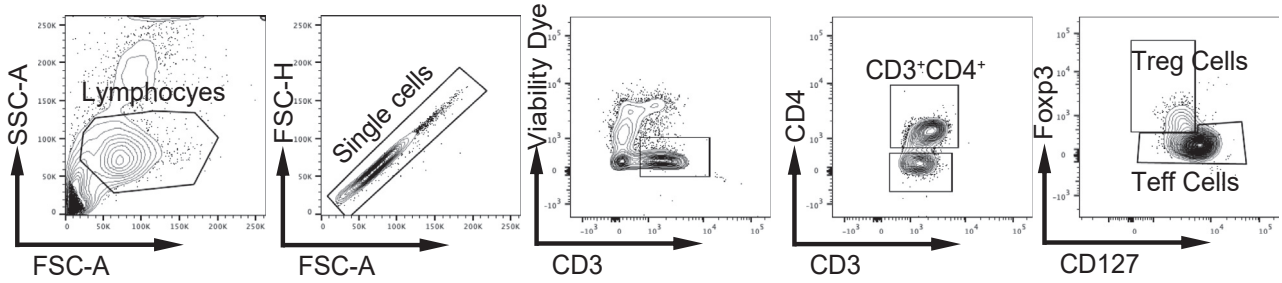


**FIG E4.** Gating strategy for T-cell subset analysis. Gating strategy for Teff and Treg cells analysis. FSC and SSC analysis of human mononuclear cells (PBMCs), followed by CD3 versus viability Dye gated on single cells, then CD3 versus CD4 gated on $CD3^+$ Viability $Dye^-$ cells and finally Foxp3 versus CD127 staining, gated on $CD3^+CD4^+$ cells.

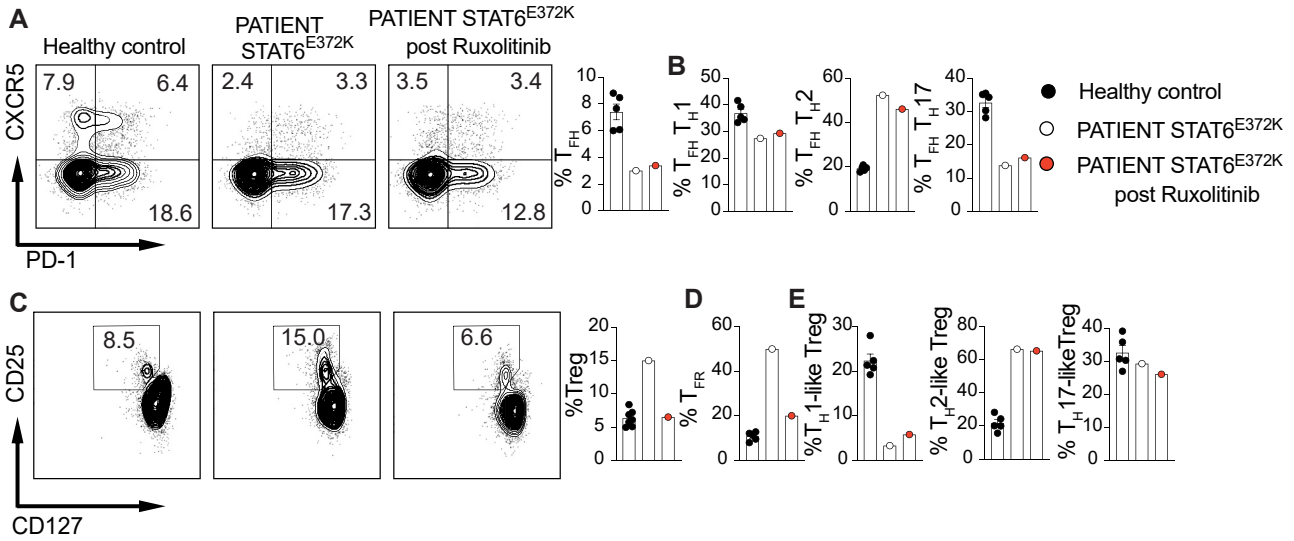


**FIG E5.** $T_{FH}$- and Treg-cell analysis in STAT6$^{E372K}$ patient pre- versus postruxolitinib treatment. **(A)** Flow cytometric and cell frequency analysis with representative plots of CXCR5$^{+}$PD1$^{+}$ CD4$^{+}$ T cells pre- and postruxolitinib compared with healthy controls. **(B)** Frequencies of $T_{FH}1$, $T_{FH}2$, and $T_{FH}17$ cells in the respective groups. **(C)** Flow cytometric and cell frequency analysis with representative plots of Treg cells pre- and postruxolitinib compared with healthy controls. **(D)** Frequencies of $T_{FR}$ cells in the respective groups. **(E)** Frequencies of $T_H1$-like Treg, $T_H2$-like Treg, and $T_H17$-like Treg cells in the respective groups. Each symbol represents one subject. Numbers in flow plots indicate percentages. Error bars indicate SEM.

**TABLE E1.** List of candidate variants identified by WES

| Genetic model | Gene name | Exonic function | Amino acid change | PolyPhen | SIFT |
|---|---|---|---|---|---|
| Recessive | *ANKRD30BL* | Nonsynonymous | p.A178V | | D |
| Recessive | *MROH5* | Nonsynonymous | p.R29Q:p.G55S | | |
| Recessive | *MADCAM1* | Nonframeshift insertion | p.S29_P30insSRHHLPGA:p.S248_P249insSRHHLPGA | | |
| Recessive | *KLF16* | Nonsynonymous | p.D14Y | D | D |
| Recessive | *MTMR1* | Nonframeshift deletion | p.H662_V665del:p.H670_V673del:p.H568_V571del | | |
| Compound-het-het | *ANXA11* | Nonsynonymous | p.R346C:p.R313C | D | D |
| Compound-het-het | *ANXA11* | Nonsynonymous | p.G19D | D | D |
| Compound-het-het | *ATM* | Nonsynonymous | p.V2079I | B | T |
| Compound-het-het | *IFNL3* | Nonsynonymous | p.E62V | D | D |
| *De novo*/dominant | *TTK* | Frameshift deletion | p.S108Mfs*6 | | |
| *De novo*/dominant | *KIAA1217* | Nonsynonymous | p.M204I:p.M407I:p.M336I:p.M486I:p.M406I | B | T |
| *De novo*/dominant | *FZD8* | Nonsynonymous | p.P170S | P | T |
| *De novo*/dominant | *ANXA11* | Nonsynonymous, splice_region | p.G19D | D | D |
| *De novo*/dominant | *SIRT3* | Nonsynonymous | p.F3S | B | D |
| *De novo*/dominant | *CHID1* | Nonsynonymous, splice_region | p.R148C:p.R118C:p.R143C | D | D |
| *De novo*/dominant | *OLFML1* | Nonsynonymous | p.I35T | D | D |
| *De novo*/dominant | *LYVE1* | Nonsynonymous | p.N185K:p.N289K | B | D |
| *De novo*/dominant | *NXPE2* | Nonsynonymous | p.Q319R | B | T |
| *De novo*/dominant | *OR8G2, OR8G2P* | Nonsynonymous | p.I89V | | |
| *De novo*/dominant | *STAT6* | Nonsynonymous | p.E262K:p.E372K | D | D |
| *De novo*/dominant | *CCDC85C* | Nonsynonymous | p.R177L | P | D |
| *De novo*/dominant | *NEDD4* | Stopgain | p.Q1095X:p.Q1151X:p.Q1167X:p.Q748X | | |
| *De novo*/dominant | *SPG21* | Nonsynonymous, splice_region | p.V76I:p.V103I | B | T |
| *De novo*/dominant | *IREB2* | Nonsynonymous | p.R697W | D | T |
| *De novo*/dominant | *DLX4* | Startloss | p.M1?:p.M1I | B | D |
| *De novo*/dominant | *CSHL1* | Nonsynonymous | p.R45H | P | T |
| *De novo*/dominant | *DDX3X* | Nonsynonymous | p.N178S:p.N194S:p.N238S | P | D |

PolyPhen and SFIT scores. Minor allele frequency ≤0.01.
*B*, Benign; *D*, deleterious; *het*, heterozygous; *P*, probably deleterious; *T*, tolerant.

**TABLE E2.** Patient scores according to the National Institute of Health–HIES scoring system

| Clinical findings | Patient's findings | Points |
|---|---|---|
| Highest serum IgE Level (IU/mL) | >2000 | 10 |
| Skin abscesses | 3-4 times | 4 |
| Pneumonia (episodes over lifetime) | 2 | 4 |
| Parenchymal lung abnormalities | Absent | 0 |
| Retained primary teeth | None | 0 |
| Scoliosis, maximum curvature | <10° | 0 |
| Fractures with minor trauma | None | 0 |
| Highest eosinophil count (cells/μL) | >800 | 6 |
| Characteristic face | Present | 5 |
| Midline anomaly | Absent | 0 |
| Newborn rush | Present | 4 |
| Eczema (worst stage) | Severe | 4 |
| Upper respiratory tract infections per year | 4-6 | 2 |
| Candidiasis | None | 0 |
| Other serious infections | None | 0 |
| Fatal infections | Absent | 0 |
| Hyperextensibility | Present | 4 |
| Lymphoma | Absent | 0 |
| Increased nasal width | 1-2 SD | 1 |
| High palate | Absent | 0 |
| Young-age correction | >5 y | 0 |
| Total score | | 44 |